General Disclaimer

One or more of the Following Statements may affect this Document

- This document has been reproduced from the best copy furnished by the organizational source. It is being released in the interest of making available as much information as possible.

- This document may contain data, which exceeds the sheet parameters. It was furnished in this condition by the organizational source and is the best copy available.

- This document may contain tone-on-tone or color graphs, charts and/or pictures, which have been reproduced in black and white.

- This document is paginated as submitted by the original source.

- Portions of this document are not fully legible due to the historical nature of some of the material. However, it is the best reproduction available from the original submission.

FWG ASSOCIATES, INC.

R. R. 2, Box 271-A
Tullahoma, TN 37388
Phone: 615/455-1982

Prepared by:

Dr. Kao-Huah Huang
Dr. Walter Frost
Mr. Erik A. Ringnes

Prepared for:

Systems Dynamics Laboratory
Atmospheric Sciences Division
NASA
Marshall Space Flight Center, AL 35812

Attn: Margaret B. Alexander/ED42

FINAL REPORT

Contract NAS8-36188
Reporting Period
Sept. 14, 1984 - May 14, 1985

COMPARISON OF WIND AND TURBULENCE MEASUREMENTS FROM DOPPLER LIDAR AND INSTRUMENTED AIRCRAFT

June 18, 1985

Approved:

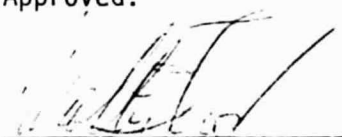

Dr. Walter Frost, President

ABSTRACT

Wind fields were measured with the ground-based NASA Marshall Space Flight Center (NASA/MSFC), Huntsville, Alabama, lidar, NOAA Wave Propagation Laboratory (NOAA/WPL), Boulder, Colorado, and with the NASA B-57B instrumented aircraft. The remotely sensed winds are compared with the *in situ* aircraft measurements. Three flight plans were carried out during the two different field programs. At NASA/MSFC the aircraft circled while the lidar scanned conically on May 10, 1983, and the aircraft flew 6° approach path along the fixed lidar beam on May 12, 1983. In Boulder, Colorado, on February 7 and 9, 1984, the aircraft flew an approach along the lidar beam directed south-north (parallel to the mountain range) and a climbout along the lidar beam which alternately shifted east-west (perpendicular to the mountain range). Turbulence intensities and spectra were calculated from the temporal fluctuations in the lidar-measured radial wind speed component. It should be noted that time histories of the lidar wind represent values spatially averaged over a 300 m volume element. The lidar winds were sampled at approximately 2 times per second whereas the aircraft measurements were sampled at 40 times per second.

The second moment or Doppler frequency spectra width of the lidar measurements was also compared with turbulence intensities measured by the aircraft. Variable sample sizes of pulses were averaged in order to resolve turbulence information from the lidar spectra width.

It is concluded that these field tests provided unique sets of data to examine the mean wind and turbulence measurements made by remote sensing instruments. The comparison of aircraft-measured turbulence intensities and spectra with lidar time histories of radial wind speed were in good agreement. Although the magnitude of lidar second moment (or spectral width) is 4 to 5 times higher than turbulence intensity, variation of the second moment does contain information representative of the actual measured turbulence.

ACKNOWLEDGMENTS

This research was supported under NASA Contract NAS8-36188. The authors are grateful for funding from the Office of Aeronautical and Space Technology, NASA Headquarters, Washington, D.C. The support of A. Richard Tobiason is acknowledged. Special thanks go to Dan Fitzjarrald and Margaret Alexander of the Systems Dynamics Laboratory, Atmospheric Sciences Division, NASA George C. Marshall Space Flight Center, Huntsville, Alabama, who monitored the research program.

TABLE OF CONTENTS

LIST OF FIGURES

1.0 INTRODUCTION

A technique of remotely sensed wind measurement was described by Huffaker et al. (1970) by applying the concept that velocity can be determined from the Doppler shift in light scattered by particles in the atmosphere (Bilbro 1980). A comparative study between a cup anemometer and a continuous wave CO_2 Laser Doppler Velocimetry (LDV) has been performed by Lawrence et al. (1972). Also, Brashears and Hallock (1976) reported the first wind profile measurement using a pulsed system. The measurements were compared with National Weather Service (NWS) wind soundings. The term "lidar" is a general term of this new remotely sensing system and is an acronym derived from light detection and ranging. One substantial improvement of wind measurement using pulsed lidar was made with the appearance of a transverse-excited atmoshperic (TEA) laser. Hall et al. (1984) reported the comparison of wind measurements using a TEA configuration lidar system and tower anemometer, rawinsonde, and the profiler. However, most comparison studies utilized a conical scanning technique known as velocity azimuth display (VAD) to resolve three-dimensional winds by using a single lidar system (Cliff and Huffaker 1974). Since the velocities determined by the VAD technique are the result of large-scale spatial averaging, the information on small-scale turbulence is lost. The lidar-measured wind and turbulence at different altitudes (range gates) have not been examined before by an in situ measurement, such as available from an instrumented aircraft. Two field tests with different comparison configurations were carried out in this regard.

The first field test was conducted at NASA Marshall Space Flight Center (NASA/MSFC) on May 10 and 12, 1983, in order to compare NASA/MSFC lidar measurements with NASA B-57B aircraft measurements. On May 10, lidar-measured winds were determined using a conical scan while the aircraft flew circular flight paths at several altitudes. On May 12, the lidar was fixed at a 6° elevation angle while the aircraft flew approach paths roughly parallel to the lidar beam. Results of the May 12 test have been presented in a previous report (Frost and Huang 1983).

The second field tests were conducted at Boulder, Colorado, on February 7 and 9, 1984. Similar to the May 12 tests, the aircraft (NASA B-57B) flew an approach along the NOAA/WPL lidar beam directed south-north (parallel to the mountain range) and a climbout along the lidar beam which shifted to an east-west (perpendicular to the mountain range) flight path.

The mean wind fields, the turbulence intensities, and the turbulence spectra determined from measurements by both systems are in good agreement. Turbulence intensities and spectra were calculated from the fluctuations with time for the lidar-measured radial wind speed component. The second moment or Doppler frequency spectra width of the lidar measurements was also compared with turbulence intensities measured by the aircraft. Variable sample sizes of pulses were averaged in order to resolve turbulence information from the lidar spectra width.

In this report, the instrumentation involved in obtaining the data and an outline of the field test plan is given in Section 2.0. In Section 3.0, the method of comparison for each of the field tests is described and the comparison and interpretation of the results from both measurements (i.e., lidar and aircraft) are also presented.

It is concluded that these field tests provided unique sets of data to examine the mean wind and turbulence measurements made by remote sensing instruments. The comparison of aircraft-measured turbulence intensities and spectra with lidar time histories of radial wind speed was good agreement. It is also concluded that the lidar second moment or Doppler lidar spectra width holds promise for being a turbulence indicator.

2.0 EXPERIMENT

2.1 Instrumentation

As mentioned previously, two field tests were carried out for this study using different lidar systems for each test. During the first field test the instrumentation consisted of the NASA/MSFC CO_2 Doppler lidar and the NASA B-57B instrumented aircraft and was conducted at NASA/MSFC, Huntsville, Alabama. The second field test was carried out at Boulder, Colorado, where the NOAA/WPL lidar system was operated to compare with NASA B-57B measurements. The instrumentation used in the first field test is discussed in a previous report (Frost and Huang 1983). Details of the NASA/MSFC Doppler lidar are also given by Bilbro and Vaughan (1978), Jeffreys and Bilbro (1975), and Lee (1982). Information on NASA's B-57B aircraft is described by Camp et al. (1983), Campbell et al. (1983), and Theon (1985). Similar to the NASA/MSFC lidar, the NOAA/WPL lidar system is also a CO_2 pulse Doppler lidar. The difference in operation between the two lidar systems are listed in Table 2.1. Details of the NSAA/WPL lidar system is provided by Post et al. (1981). The main difference between the systems is their configuration. The configuration of the NASA/MSFC pulse lidar is a master oscillator power amplifier (MOPA), while NOAA/WPL pulse lidar is a hybrid, transverse-excited atmosphere (TEA) configuration. One shortcoming of the MOPA configuration is the relatively low per-pulse energy, typically 10 to 30 mJ (Bilbro 1980). It takes at least 50 pulses to obtain a meaningful velocity measurement. Moreover, it is poor as a second moment (spectral) estimator, due to the signal-to-noise ratio (SNR) being low. These deficiencies have been improved substantially by the TEA laser system. The TEA laser which is used at NOAA/WPL, produces 100 mJ of energy at a 12 Hz rate, which provides sufficient frequency stability to allow wind velocity measurement, and also to give meaningful output as a second moment estimator.

2.2 Field Test Design

This report emphasizes the data from the NASA/MSFC May 10, 1983, test and the NOAA/WPL field tests of February 7 and 9, 1984. During the

TABLE 2.1. Comparison of the Lidar System Parameters Between NASA and NOAA Lidar.

Parameter	NASA/MSFC	NOAA/WPL
Source	CO_2	CO_2
Wavelength	10.6 μm	10.6 μm
Configuration	MOPA	TEA
Pulse Energy	25 mJ	100 mJ
Pulse Duration	2 μs	2 μs
Pulse Per Second	110 pps	12 pps
Number of Pulse Averaged	50	6, 24, or 48

field test of May 10, 1983, the Doppler lidar was operated in a conical scanning mode, or the velocity azimuth display (VAD) mode. Scans were carried out at elevation angles of 6°, 9°, 13°, 19°, 26°, and 32°. The aircraft flew circular flight paths at increasing altitudes in order to approximately capture the lidar beam as illustrated in Figure 2.1. Figure 2.2 shows one circle of a VAD at the 6° elevation angle. Each vector shown in Figure 2.2 represents the radial component of wind velocity. The mean wind direction can be detected as roughly 200 ±20° from the plot. Wind velocity data of four different runs (Runs 13, 15, 18, and 20) from aircraft measurements are also available. Table 2.2 lists the altitudes and mean radii for the circular patterns of the aircraft trajectories. Based on the aircraft altitude, the range gate for the corresponding altitude was selected for each run in order to compare the two measurements. Figure 2.3 shows the horizontal wind vector of the aircraft measurement for Run 13 at an altitude of 592 m above mean sea level (MSL). The mean wind direction is also in the range of 200° to 240°. The NASA/MSFC tower measurements (Figure 2.4), which were obtained just before taking the measurements used in the lidar and aircraft comparison study, also shows similar direction at 187 m MSL (20 m above local terrain). The figure clearly indicated that the mean wind direction approaches 200° near the end of the time period over which the measurement was made. This is in agreement with both lidar and aircraft measurements at higher altitudes.

The second field test was conducted at Boulder, Colorado. The NOAA/WPL lidar was located on the northeastern corner of Table Mountain. On both test days (i.e., February 7 and 9, 1984), the lidar was fixed at a 4.5° elevation angle for both the 200° and 290° azimuthal from true north. The aircraft flew an approach (slope approximately 4.5°) into the lidar beam directed at 200° azimuth (roughly parallel to the mountain range) and a climbout along the lidar beam which shifted to an azimuth of 290° (roughly perpendicular to the mountain range). Figure 2.5 shows the lidar beam location relative to the terrain. The synoptic flow patterns of both test days are different. The prevailing wind direction was 30° from true north (parallel to the mountain range) on

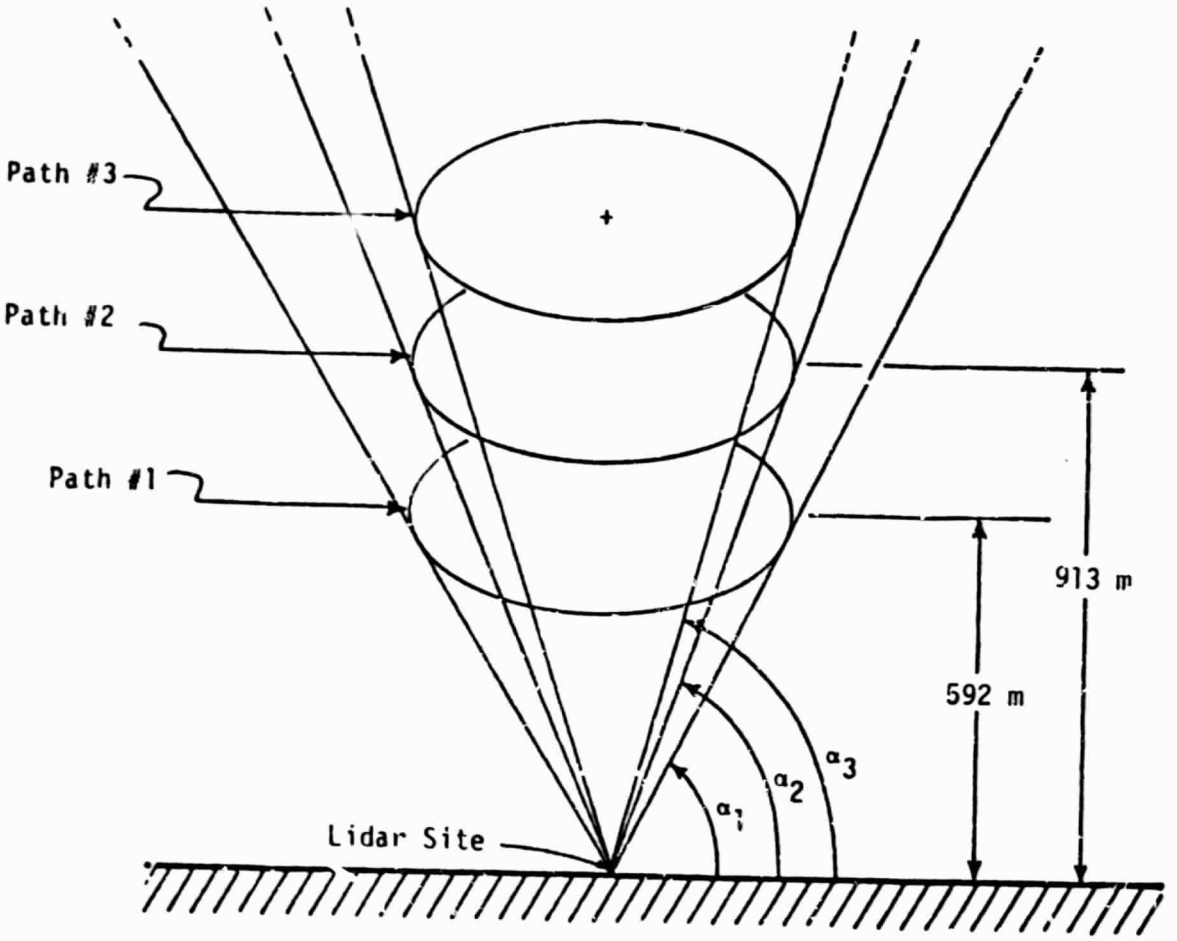

Figure 2.1. May 10, 1983: B-57B flight path.

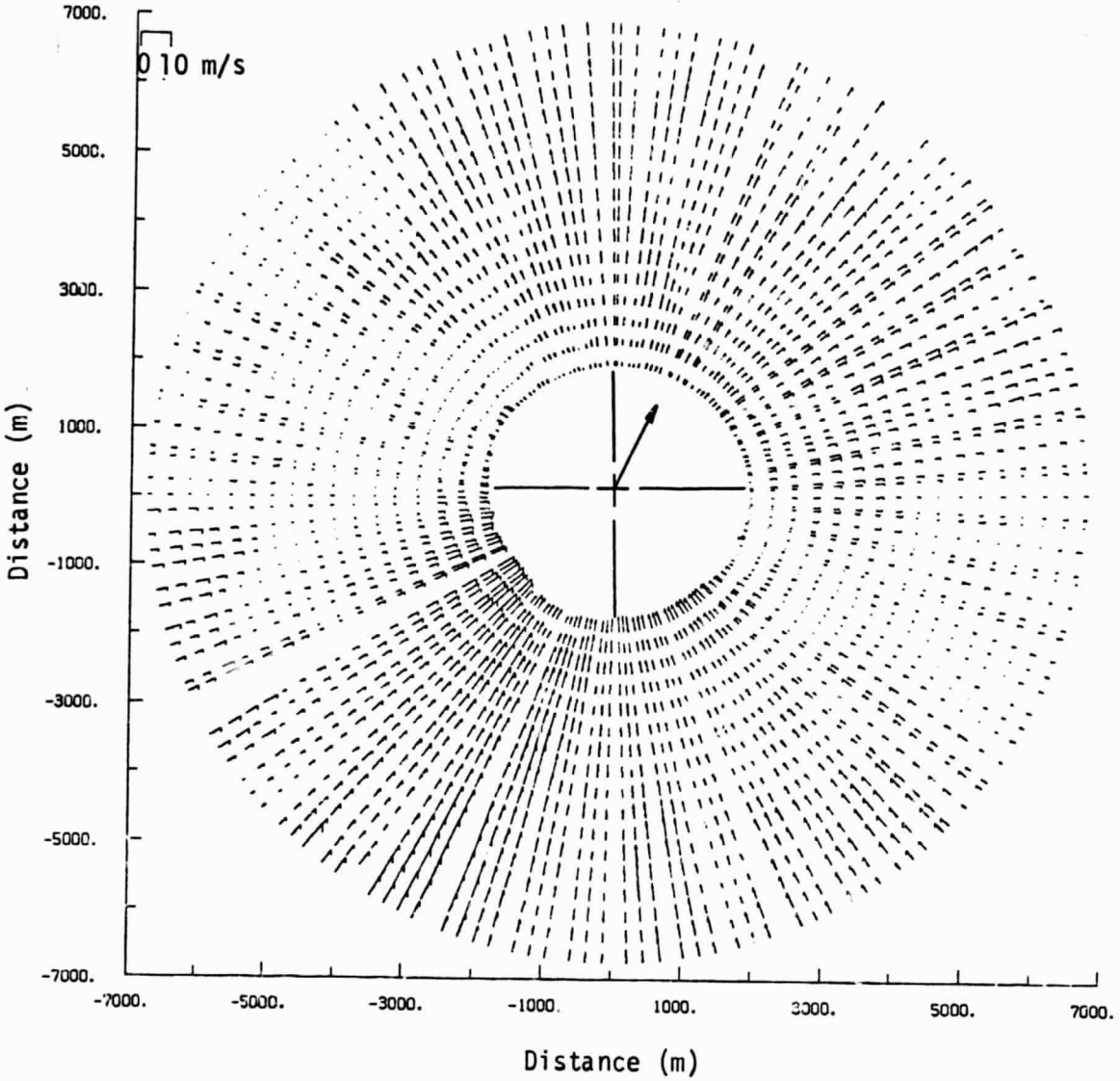

Figure 2.2. Radial wind vectors of lidar measurement from range gates 6 to 30 scanning 360° at 6° elevation angle.

TABLE 2.2. Comparison of B-57B and Lidar Data.

Flight 40 Run No.	B-57B Mean Radius (m)	B-57B Altitude MSL (m)	Time (sec)	Lidar Elevation Angle (deg)	Lidar Range Gate No.	Lidar Mean Radius (m)
13	4,400	592	350	6	14	3,920
15	4,500	913	371	9	17	4,628
18	5,120	1,226	340	13	16	4,530
20	5,100	1,834	353	19	17	4,803

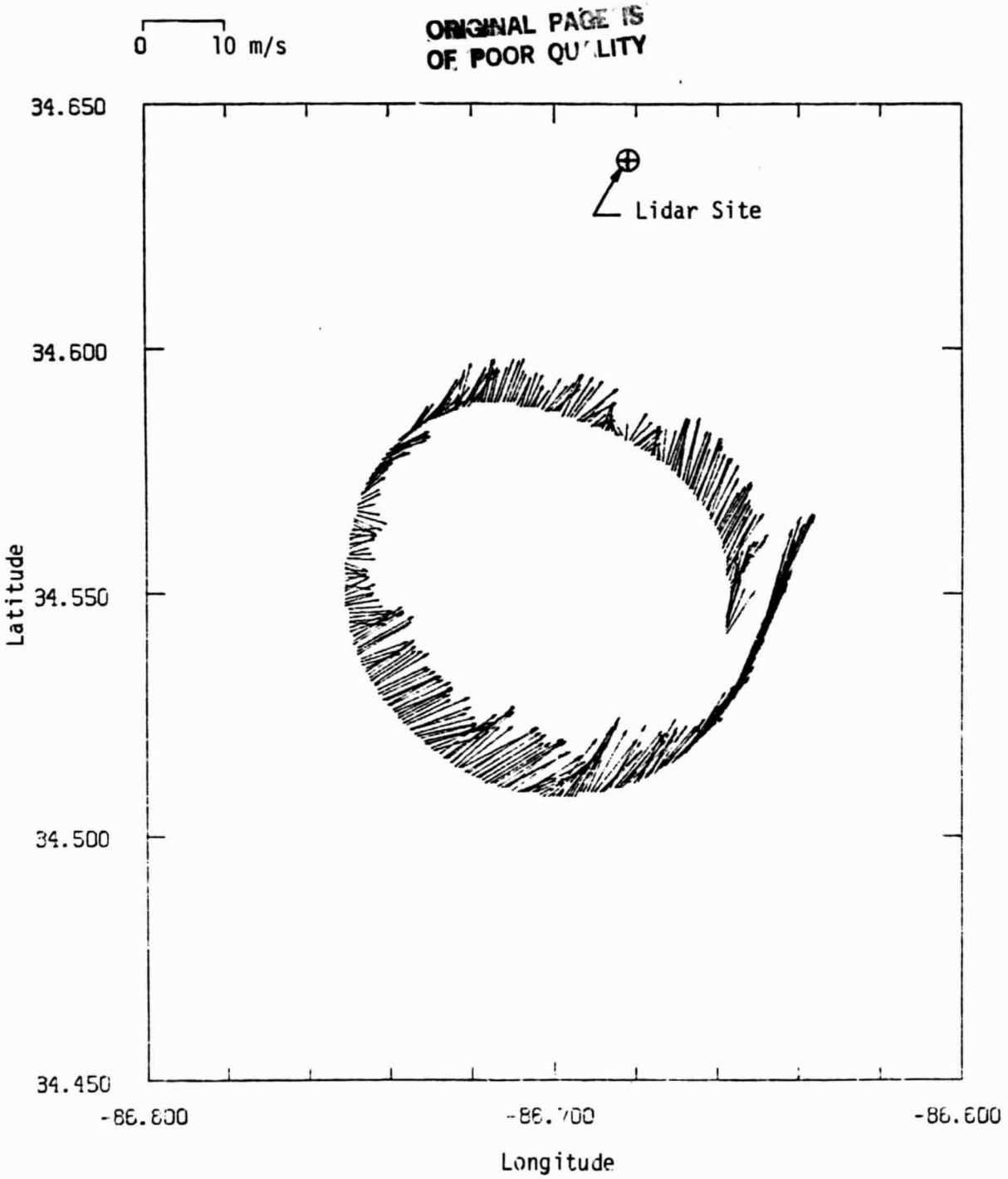

Figure 2.3. Horizontal winds along the B-57B flight pattern; Run 13, May 10, 1983, at NASA/MSFC.

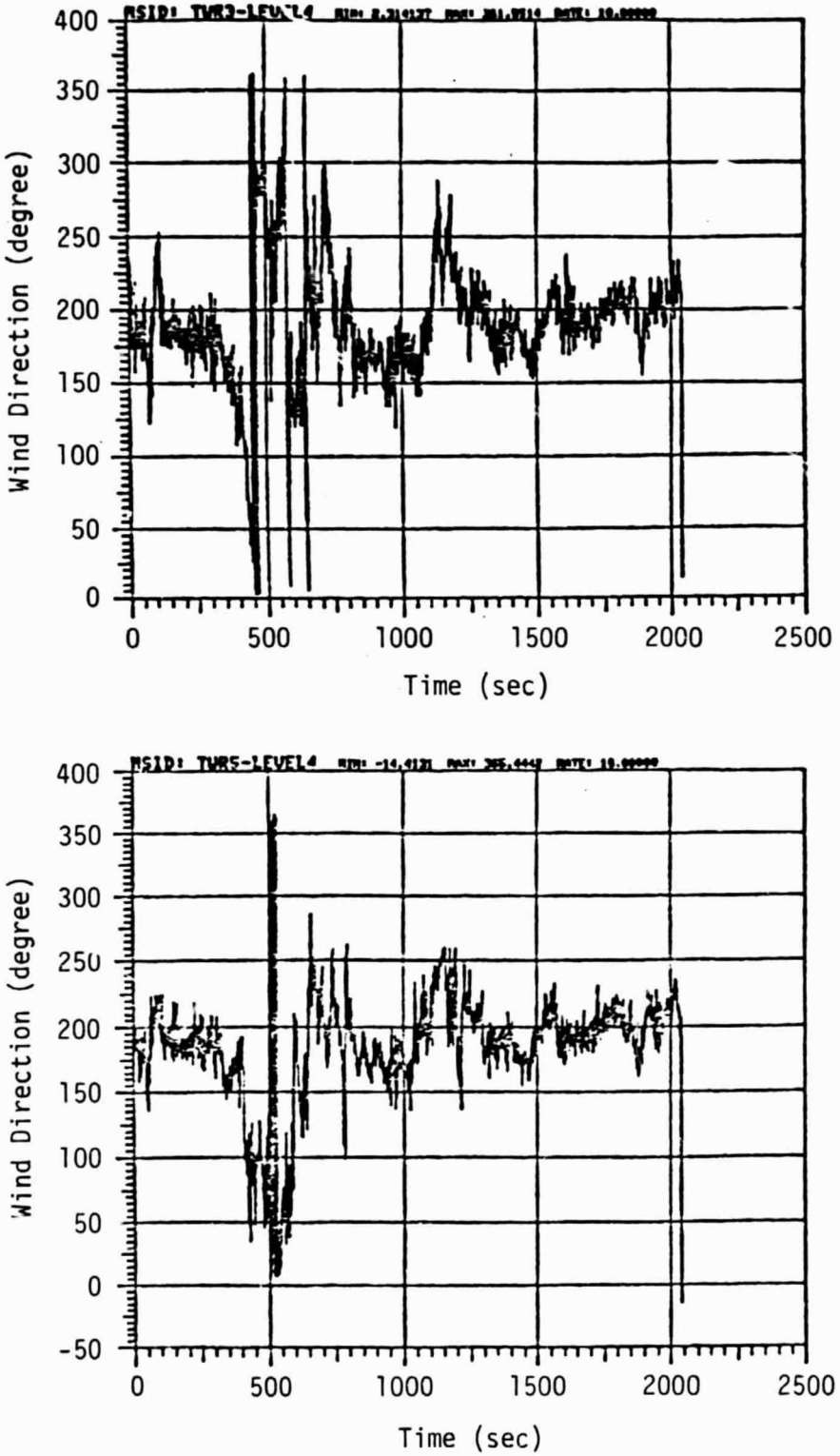

Figure 2.4. Wind direction measured on two towers for the May 10, 1983, data at the 20 m level (187 m MSL).

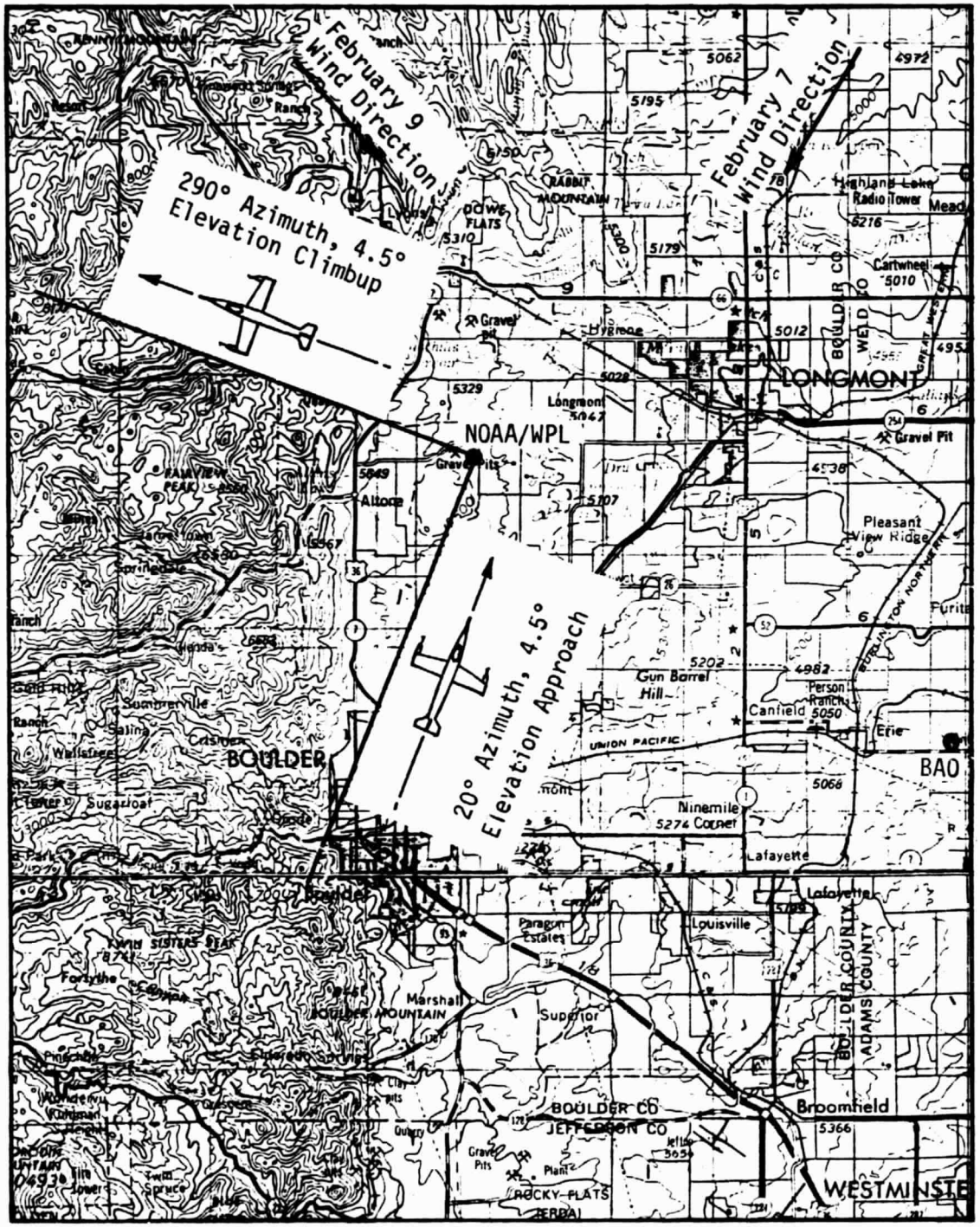

Figure 2.5. Two fixed lidar beams (200° and 290° azimuth) relative to the contour at Boulder, Colorado.

February 7 while it was 310° (oblique relative to the mountain range) on February 9. For the flow oblique relative to the mountain range, the general flow pattern is more like a vortex shed from a ridge of the mountain range. This is similar to a flow approaching a fence at an oblique angle. Figure 2.6 schematically illustrates a vortex flow pattern while Figure 2.7 shows how laboratory wind tunnel simulations have identified vortex flow off the Rock of Gibraltar (Cook et al. 1978).

Figure 2.8 shows the time histories of radial wind component which was measured at 290° azimuth on February 9. It clearly shows the reverse flow associated with the vortex flow at lower altitudes. Detailed analysis of the data and comparison of both measurements will be discussed in Section 3.0.

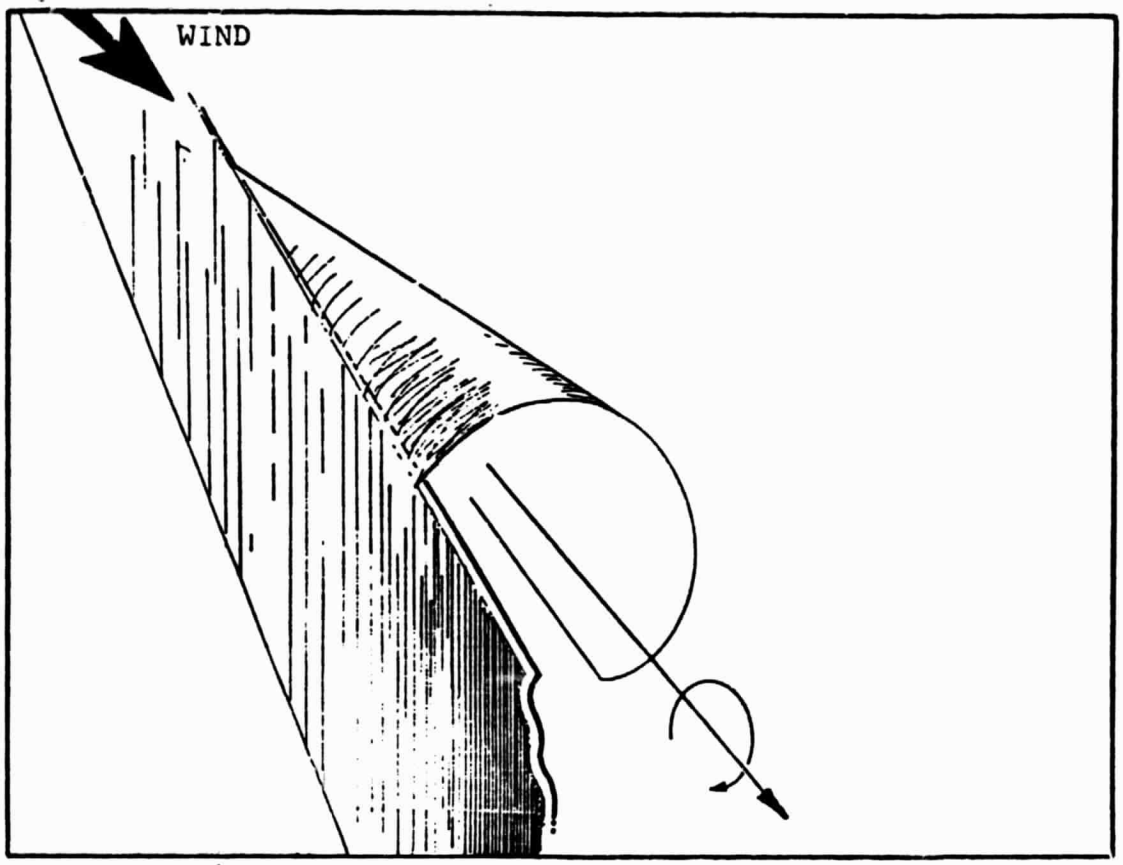

Figure 2.6. Illustration of leading edge vortex due to oblique flow over a long fence or ridge.

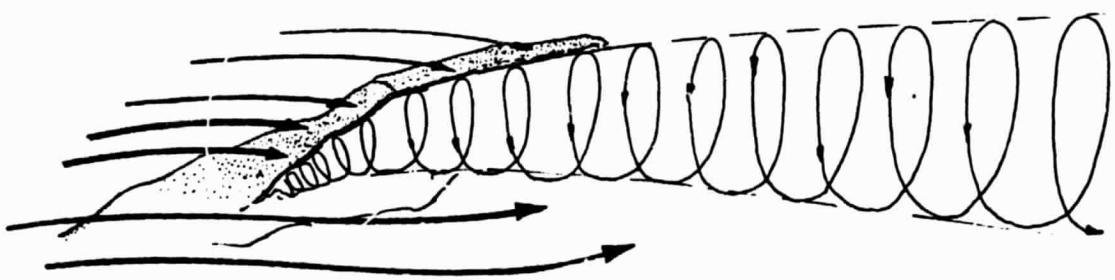

Figure 2.7. Wind tunnel observation of the vortex for wind from 200° true north at the Rock of Gibraltar (Cook et al. 1978).

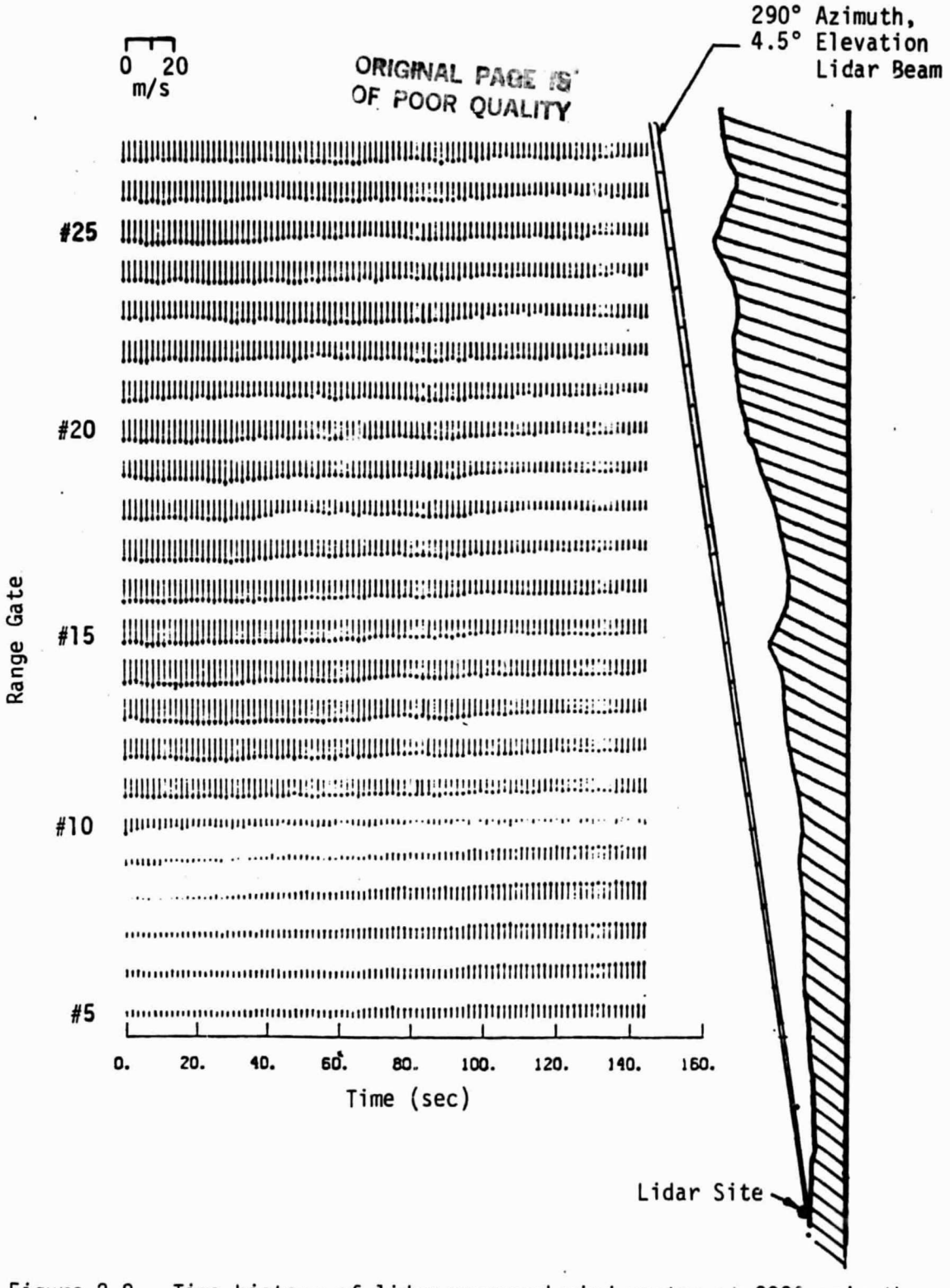

Figure 2.8. Time history of lidar-measured wind vector at 290° azimuth, 4.5° elevation relative to the terrain on February 9, 1984, Boulder, Colorado.

3.0 COMPARISON OF LIDAR MEASUREMENTS WITH AIRCRAFT MEASUREMENTS

Since the study was to compare Doppler lidar-measured winds and turbulence with *in situ* aircraft measurements and since the instrument orientations of both measurements are different, the aircraft data were reconstructed according to the lidar beam configuration for each field test. It is also necessary to assure that *in situ* measurements were compared with lidar measurements at corresponding time and spatial positions. In this section, results from the May 10 data will be discussed first. An investigation of correlation between lidar amplitude and turbulence intensities is then given, and finally results for the February 1984 field test are presented.

3.1 NASA/MSFC Field Test

As indicated in Table 2.2, it takes 6 minutes for the aircraft to complete a 9000 m diameter circle. Figure 3.1 shows the one-second average horizontal wind vectors measured by the aircraft. A total of four runs at different altitudes are presented in this figure. The figure shows the spatial wind variation at each level and also a mean wind velocity increase with altitude. These wind vectors were plotted according to the longitude and latitude coordinates which were recorded on the flight data tape. An error in the aircraft's inertial navigation system (INS) was encountered during the flight tests. The aircraft's longitude and latitude data indicate the lidar site is not enclosed in the circular pattern, which in fact is not the case. Evidence of INS problems was also shown for the May 12 test (Frost and Huang 1983). In order to compare with the lidar measurements, these circular patterns were shifted such that the centers of these circles were at the lidar site and in accord with visual observations. As shown in Figure 2.2, the lidar-measured wind is the radial component along each range gate for given elevation and azimuth angles. However, the recorded aircraft measurements are the three components (east-west wind, W_E, north-south wind, W_N, and vertical wind, W_Z) of wind velocity at the aircraft's

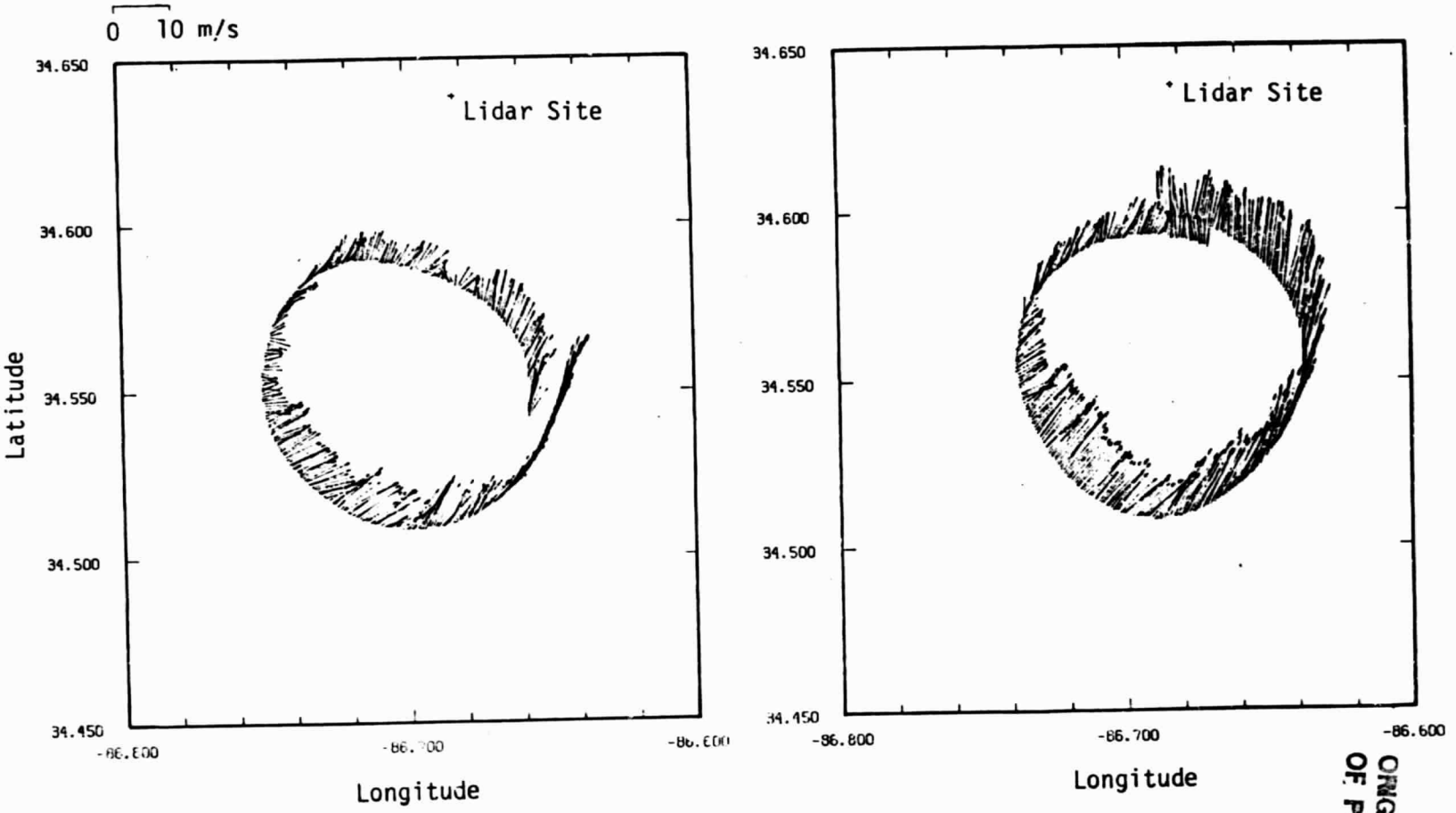

(a) Run 13, h = 592 m

(b) Run 15, h = 913 m

Figure 3.1. Aircraft-measured horizontal mean wind vector.

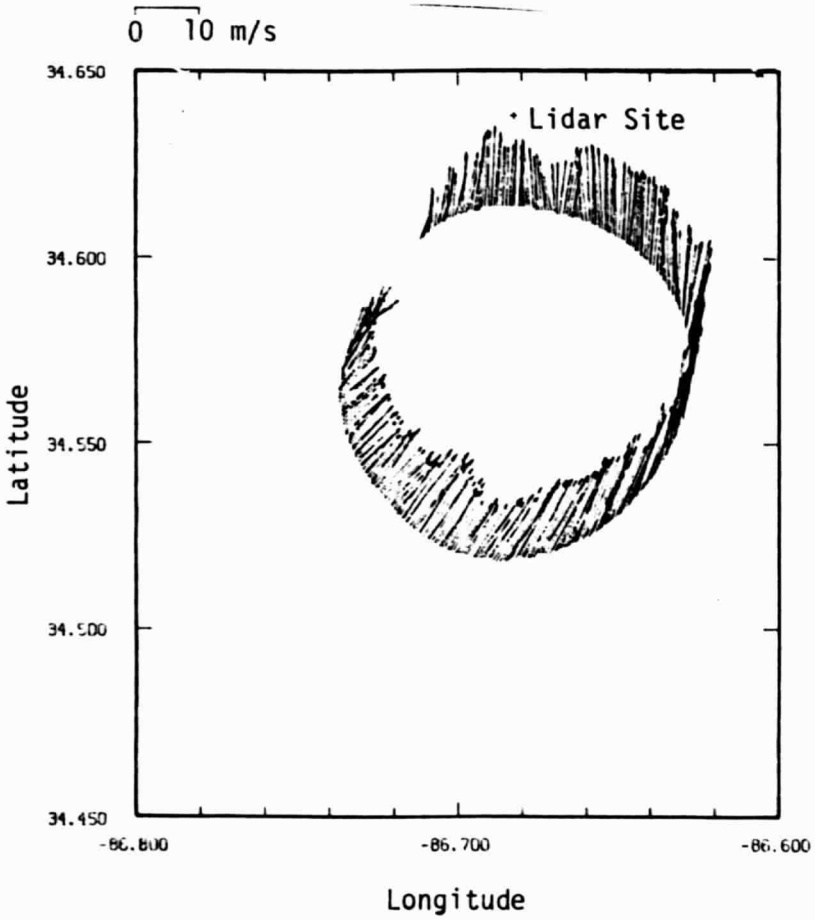

(c) Run 18, h = 1226 m

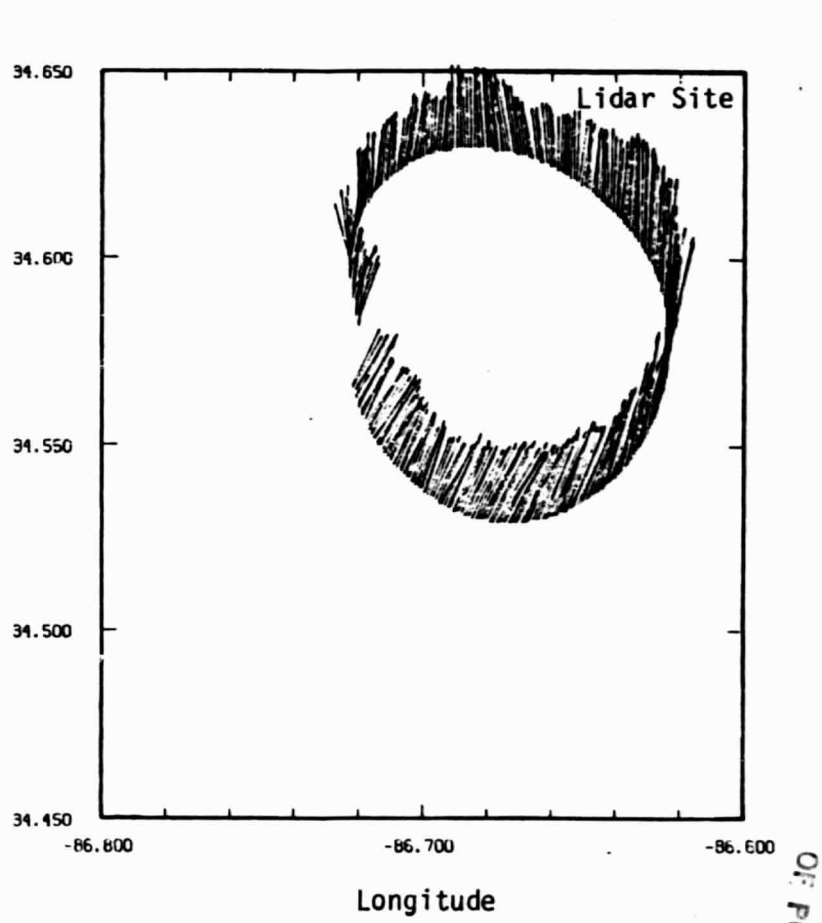

(d) Run 20, h = 1834 m

Figure 3.1. (continued).

position in the earth coordinate system, as shown in Figure 3.2. The radial component of the aircraft measurement, W_R, was computed according to the following equation:

$$W_R = (W_E \sin \phi + W_N \cos \phi) \cos \theta + W_Z \sin \theta$$

where ϕ is the azimuth angle and θ is the elevation angle. Both ϕ and θ can be calculated using the longitude and latitude data of the aircraft relative to the coordinates of the lidar site. Radial components of lidar measured wind at the range gate which was located at the aircraft altitude were then selected for comparison with the in situ measurements. The corresponding gate numbers are given in Table 2.2.

Figure 3.3 shows a comparison of mean radial wind speed from the lidar and aircraft measurements. Since the sampling rate of the aircraft measurements is 40 Hz, and it takes 6 minutes to complete one circle, the output data for one run is roughly 17,000 data points. The sample rate of the lidar is 2 Hz, and it takes 75 seconds to complete one circle, thus 150 data points were collected for each 360° scan. Although both measurements are very nearly at the same altitude, the sampling volumes could be separated by 100 m to 500 m as estimated for the circle radii (see Table 2.2). These effects may explain the difference between the two measurements. Generally speaking, however, agreement between the aircraft and the lidar radial mean velocity components is good. Both measurements show the same range of mean wind direction between 200° to 240°. The spike seen in the lidar measurement in these figures is believed to be caused by a reflection of the lidar beam from a meteorological tower near the lidar site.

Since the lidar scanned conically, the radial component of wind velocity appears to have a sinusoidal shape as shown in Figure 3.3. For a given altitude (or range gate), if the wind direction and speed are constant, the radial wind component must be a perfect sinusoidal curve. A sine curve was fit to each data set. The difference between the radial mean wind and the sinusoidal curve fit is taken as the radial turbulence component. Figure 3.4 shows the original radial wind velocity

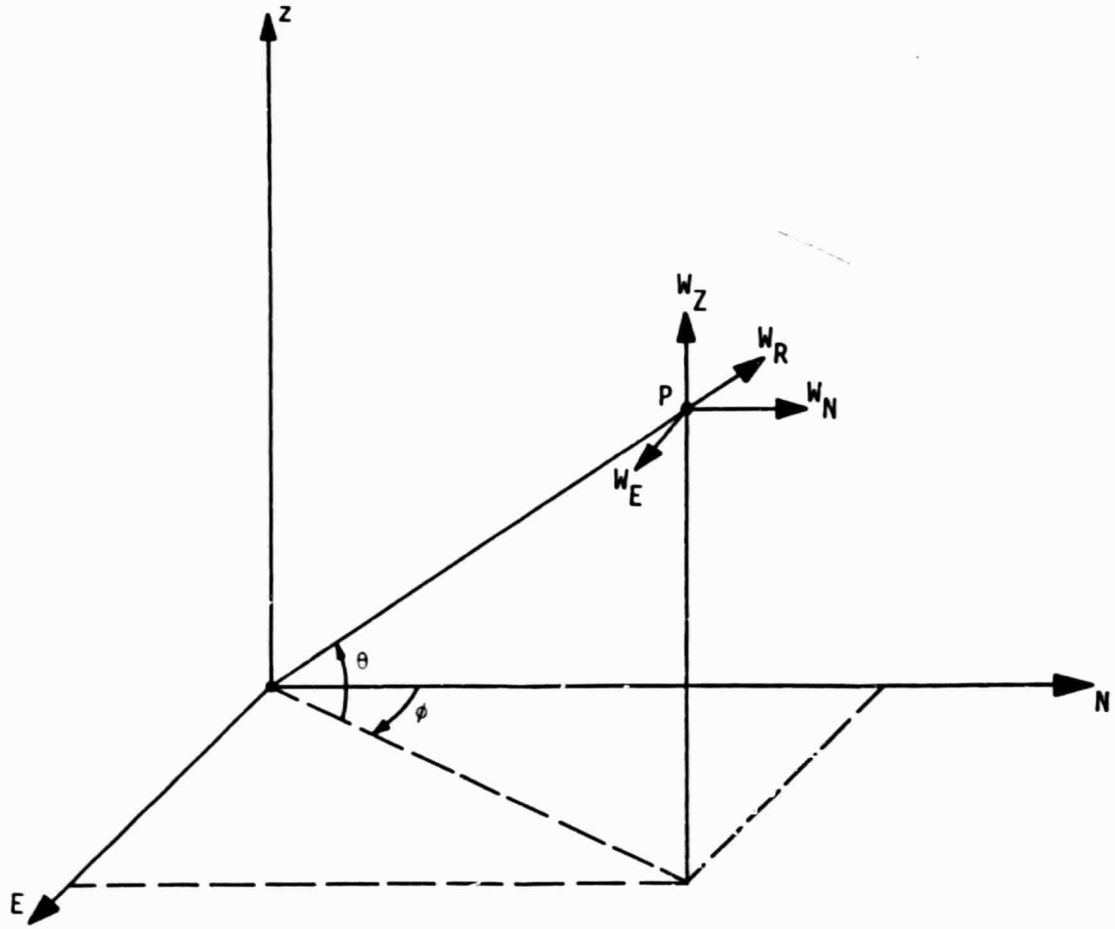

Figure 3.2. Coordinate system for transfering the aircraft-measured wind into radial component.

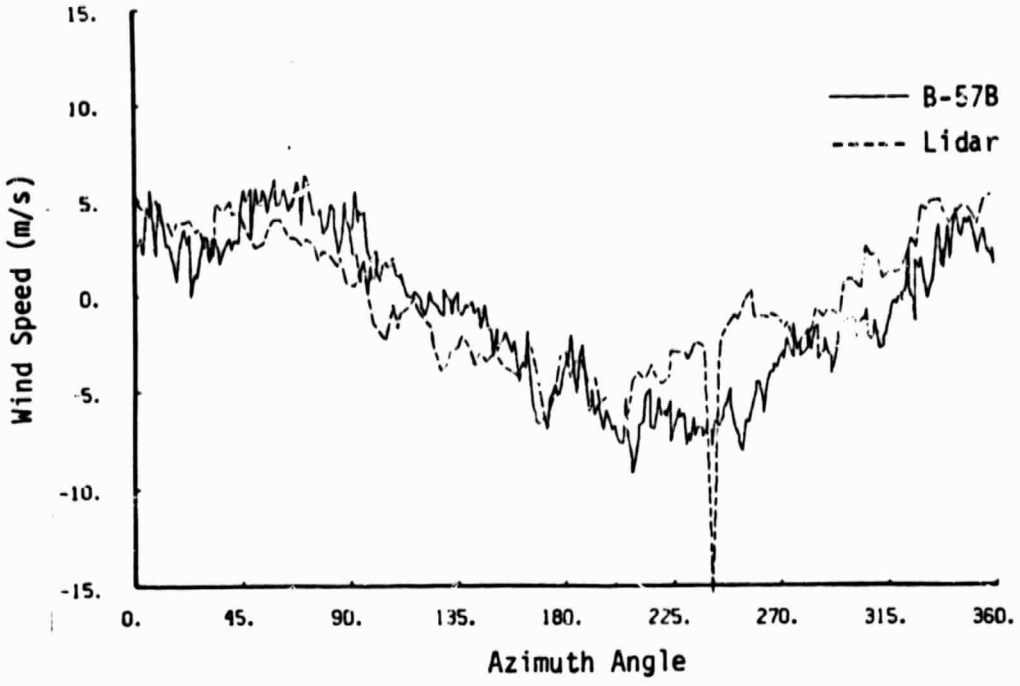

(a) Run 13, h = 592 m MSL

(b) Run 15, h = 913 m MSL

Figure 3.3. Comparison of radial wind speeds between aircraft and lidar measurements.

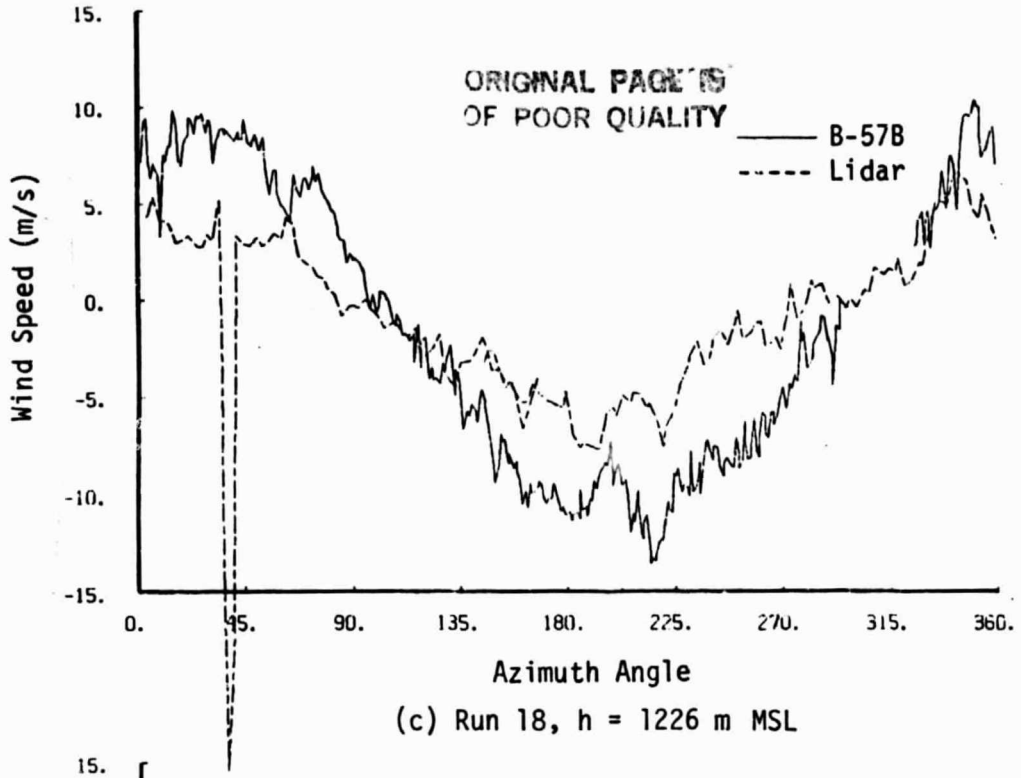

(c) Run 18, h = 1226 m MSL

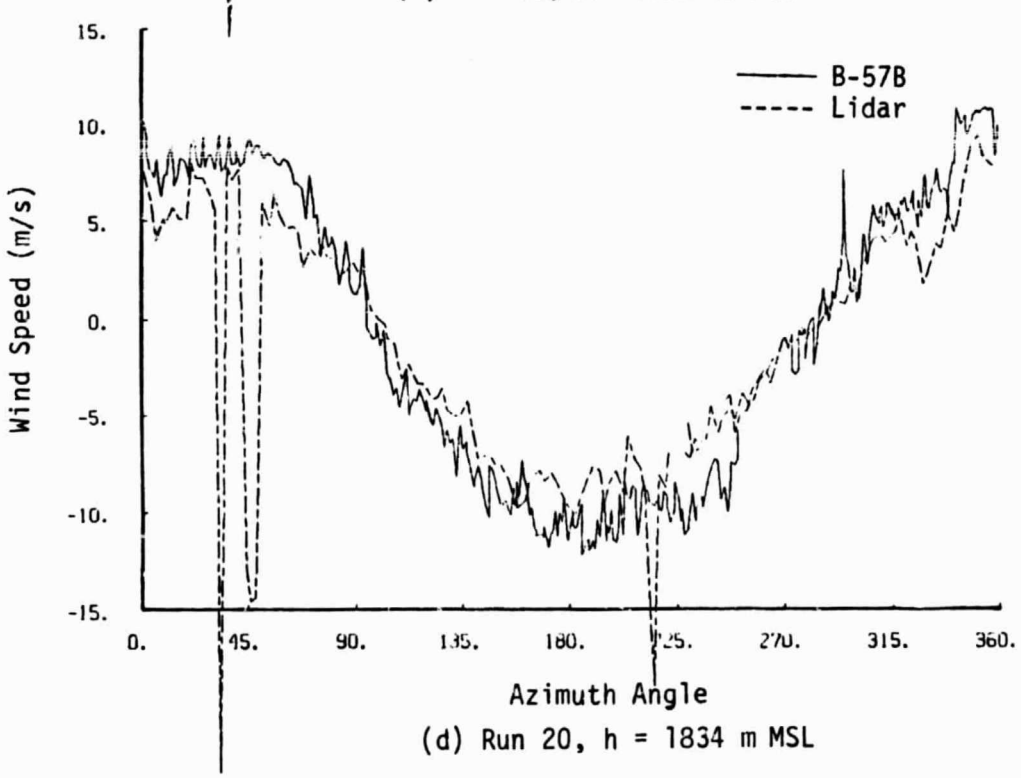

(d) Run 20, h = 1834 m MSL

Figure 3.3. (continued).

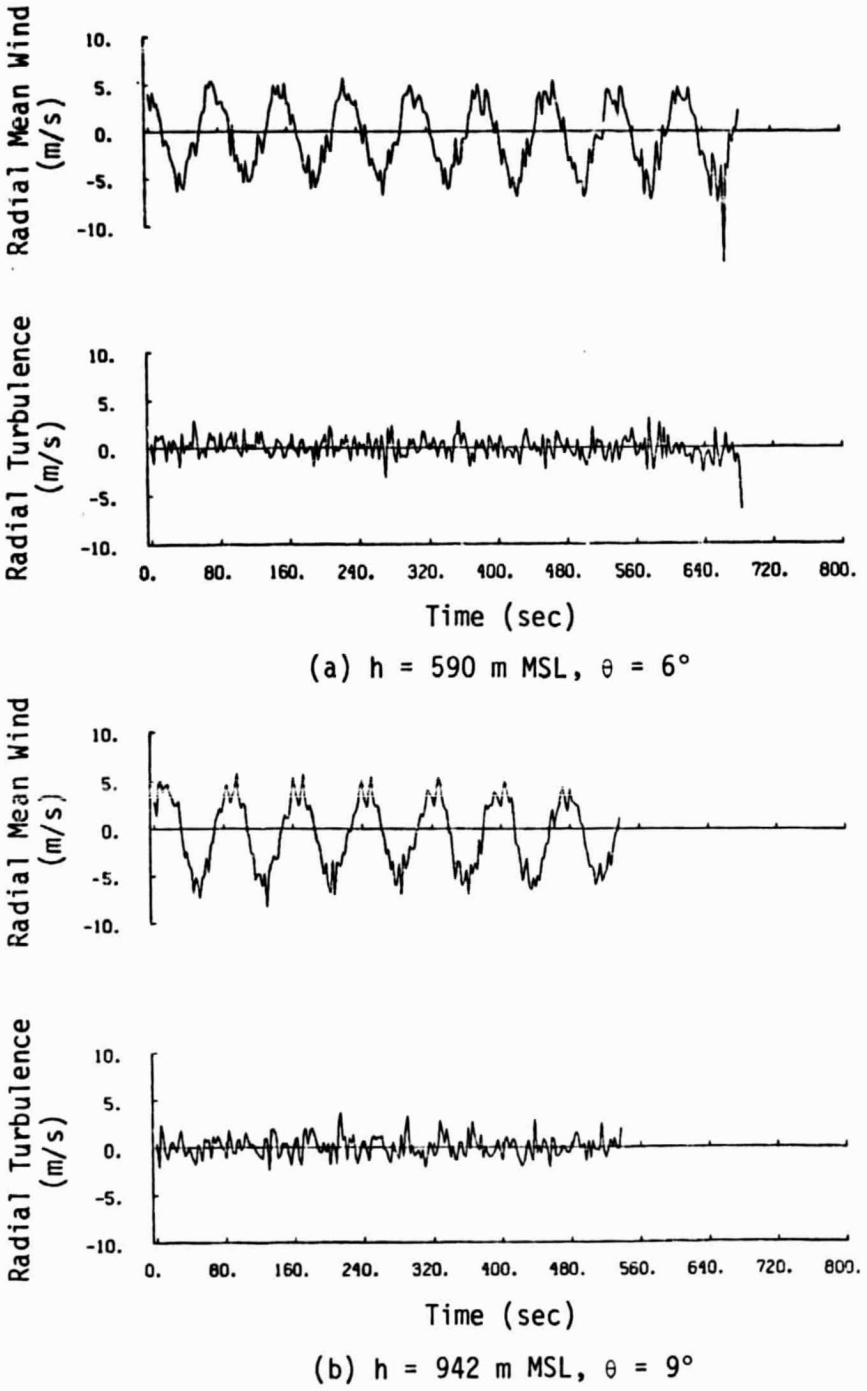

Figure 3.4. Time histories of lidar-measured wind velocity and its turbulence component at different runs.

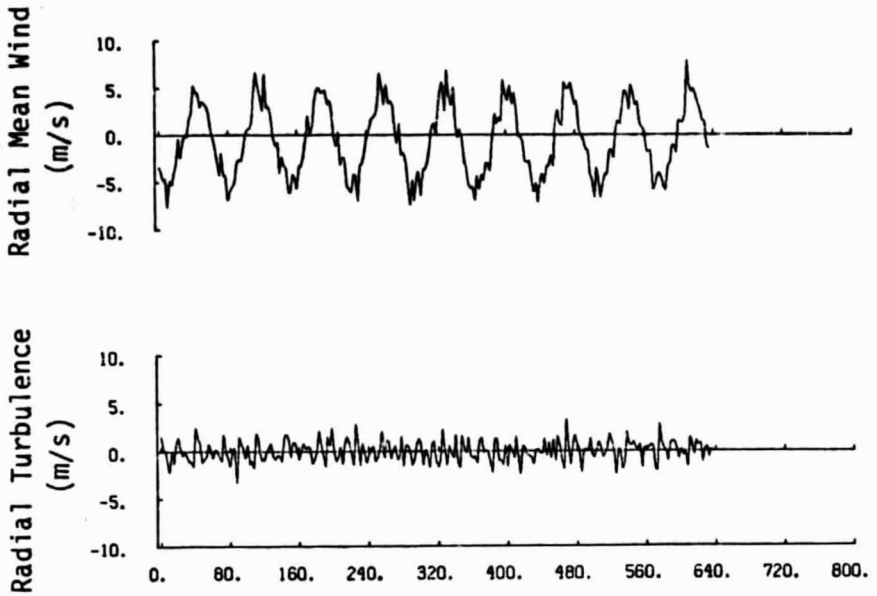

(c) h = 1213 m MSL, θ = 13°

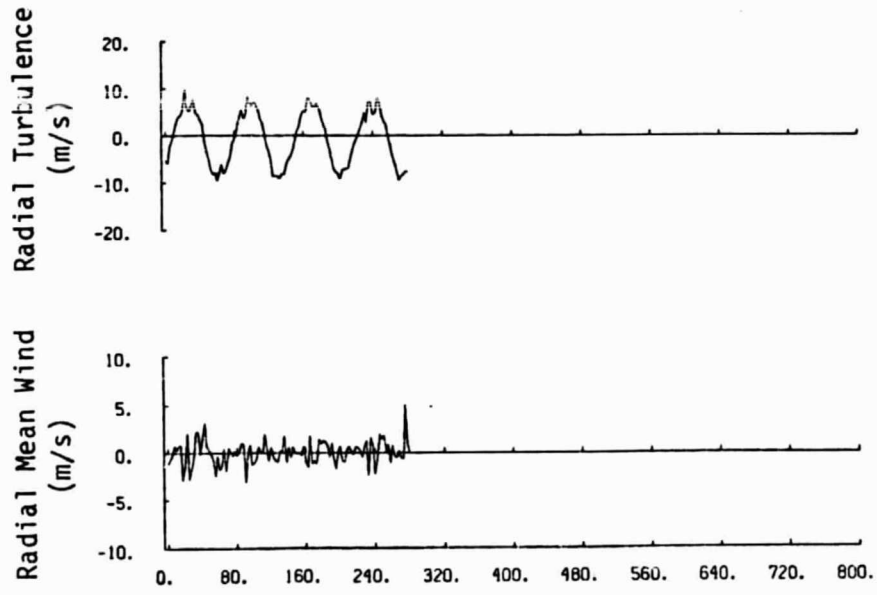

(d) h = 1877 m MSL, θ = 19°

Figure 3.4. (continued).

and the turbulence component after a sinusoidal curve fit has been removed.

Similarly the radial turbulence component of the aircraft measurements can be extracted from the radial wind velocity as shown in Figure 3.5. Since the aircraft flew only one circle for each run, only one period of a sinusoidal curve needs to be removed. With the time histories of the turbulence component resolved in the preceding manner, the turbulence intensity can be calculated. Figure 3.6 shows the turbulence intensity at different altitudes along with the mean radial velocity for given mean wind directions for both measurements. The wind speed profile contains 2 to 3 m/s difference, while the turbulence intensity shows 0.3 to 0.5 m/s difference between the aircraft and lidar measurements. The fact that the magnitude of aircraft-measured wind is 2 to 3 m/s higher than lidar-measured wind most of the time might be partially attributed to the Schuler frequency of the aircraft navigation system. A detailed investigaton of this is recommended. The comparison of lidar second moment (spectral width) with aircraft-measured turbulence intensity is not possible since the lidar second moment data is not meaningful at the altitude for which aircraft measurements were made.

In order to investigate the turbulence measurements further, the turbulence energy spectra were computed. The spectra from aircraft-measured turbulence were computed by averaging ten segments of the time record, each segment contained 1024 data points. The spectra of lidar-measured turbulence, on the other hand, were computed by averaging 4 to 8 segments of the time history, each segment containing a total of 128 points. The results are shown in Figure 3.7. Since different sampling rates are involved, the spectra distributions of lidar-measured turbulence cover a range of 0.01 Hz to 1 Hz, while spectra of aircraft-measured turbulence cover from 0.04 Hz to 20 Hz. The spectra distributions of both measurements agree well in the frequency band where they overlap, except at the highest measurement level, $\theta = 19°$. The deviation of the lidar turbulence spectra at this level from the aircraft turbulence spectra may be due to the length of lidar data time recorder being too

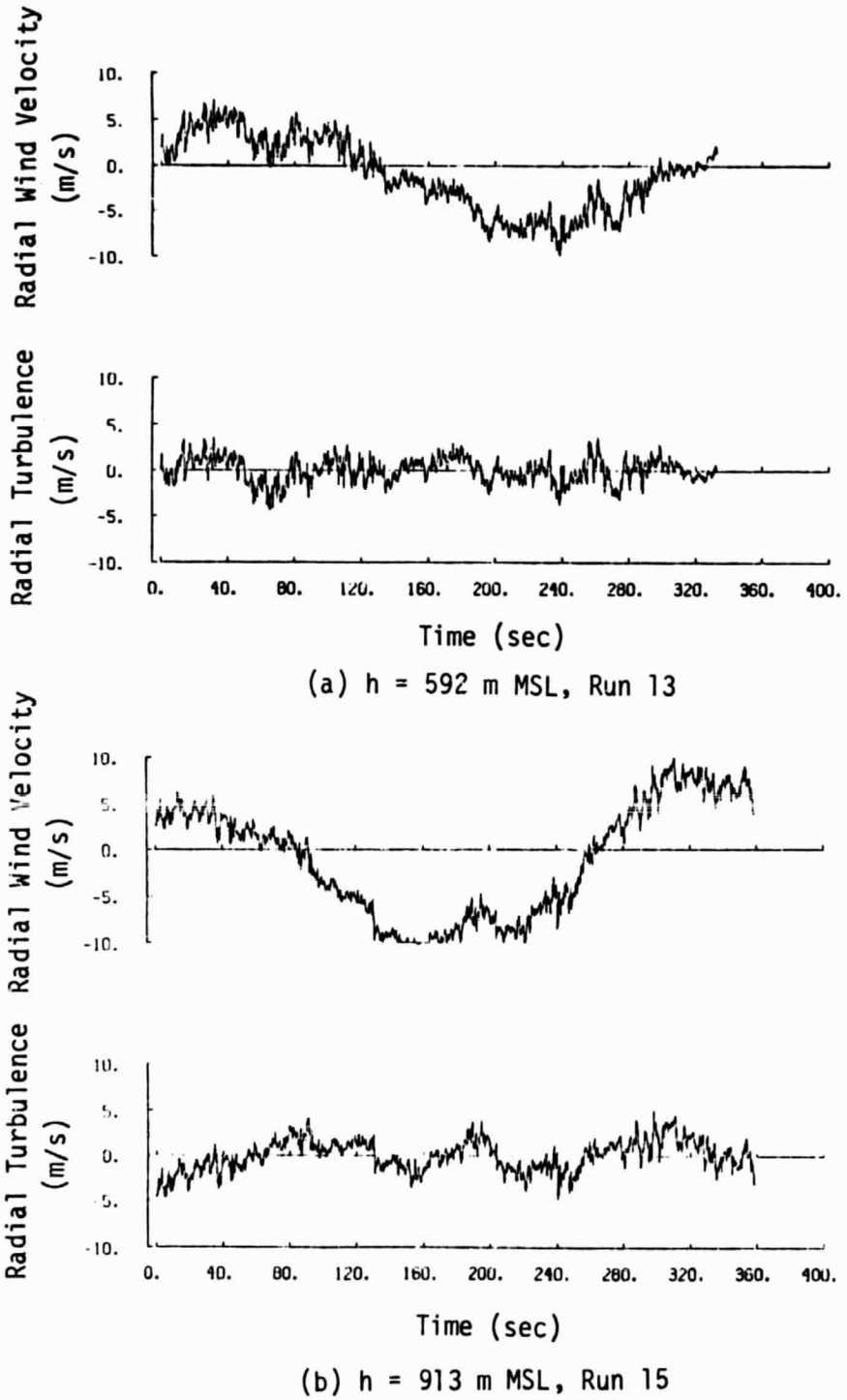

Figure 3.5. Time histories of aircraft-measured radial wind velocity and its turbulence component at different runs.

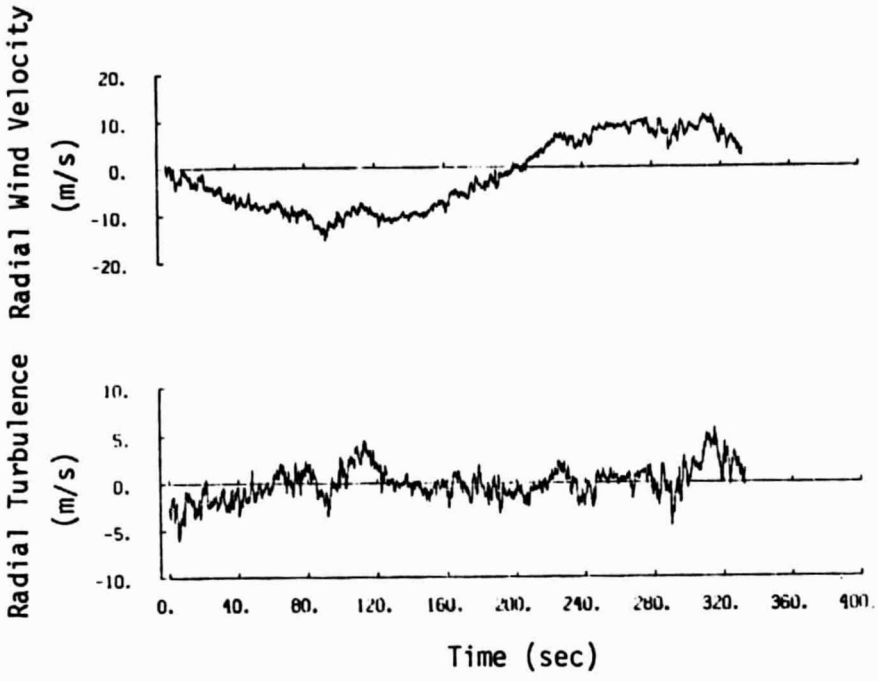

(c) h = 1226 m MSL, Run 18

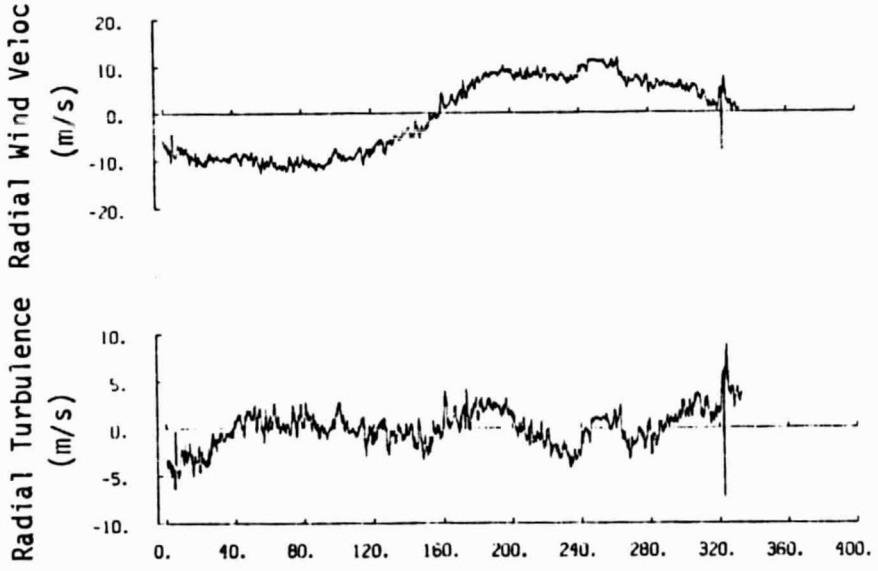

(d) h = 1834 m MSL, Run 20

Figure 3.5. (continued).

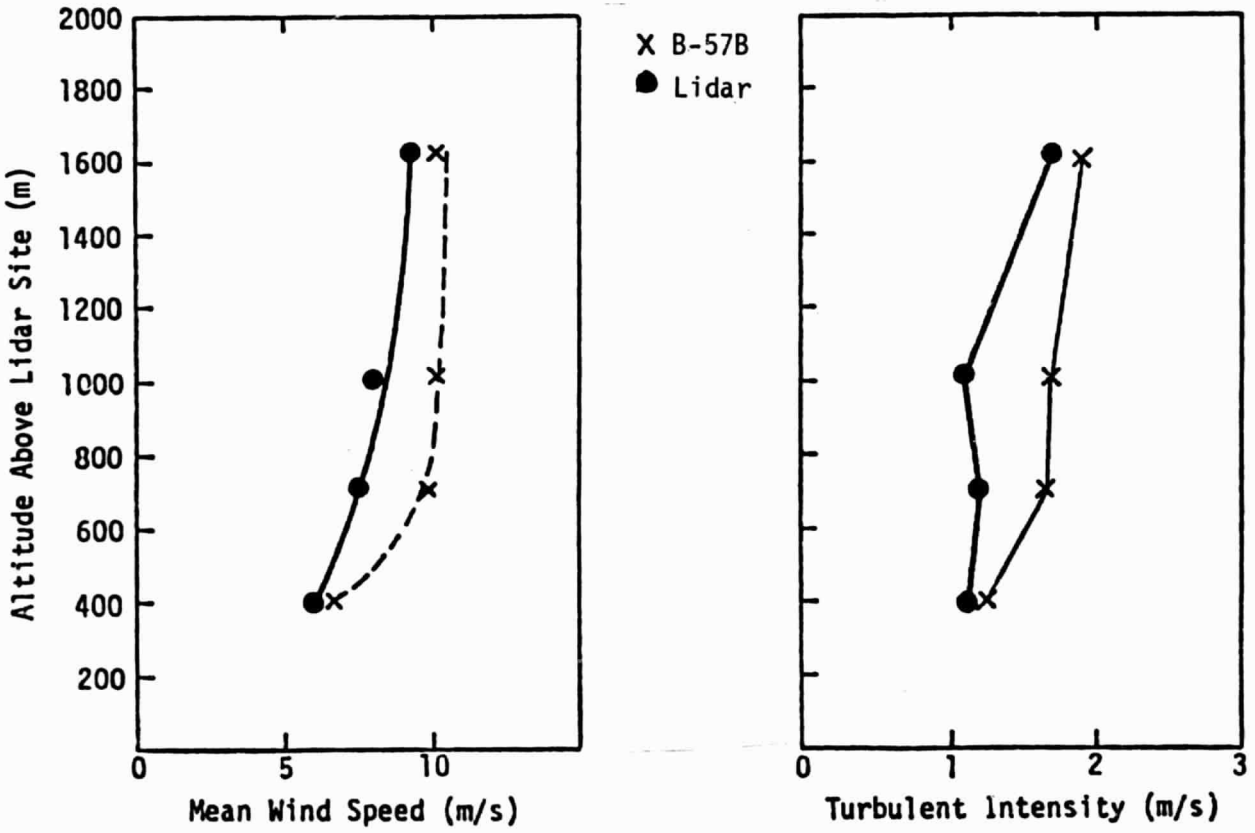

Figure 6. Comparison of radial mean wind speed at mean wind direction and calculated turbulence intensity between lidar and aircraft measurements.

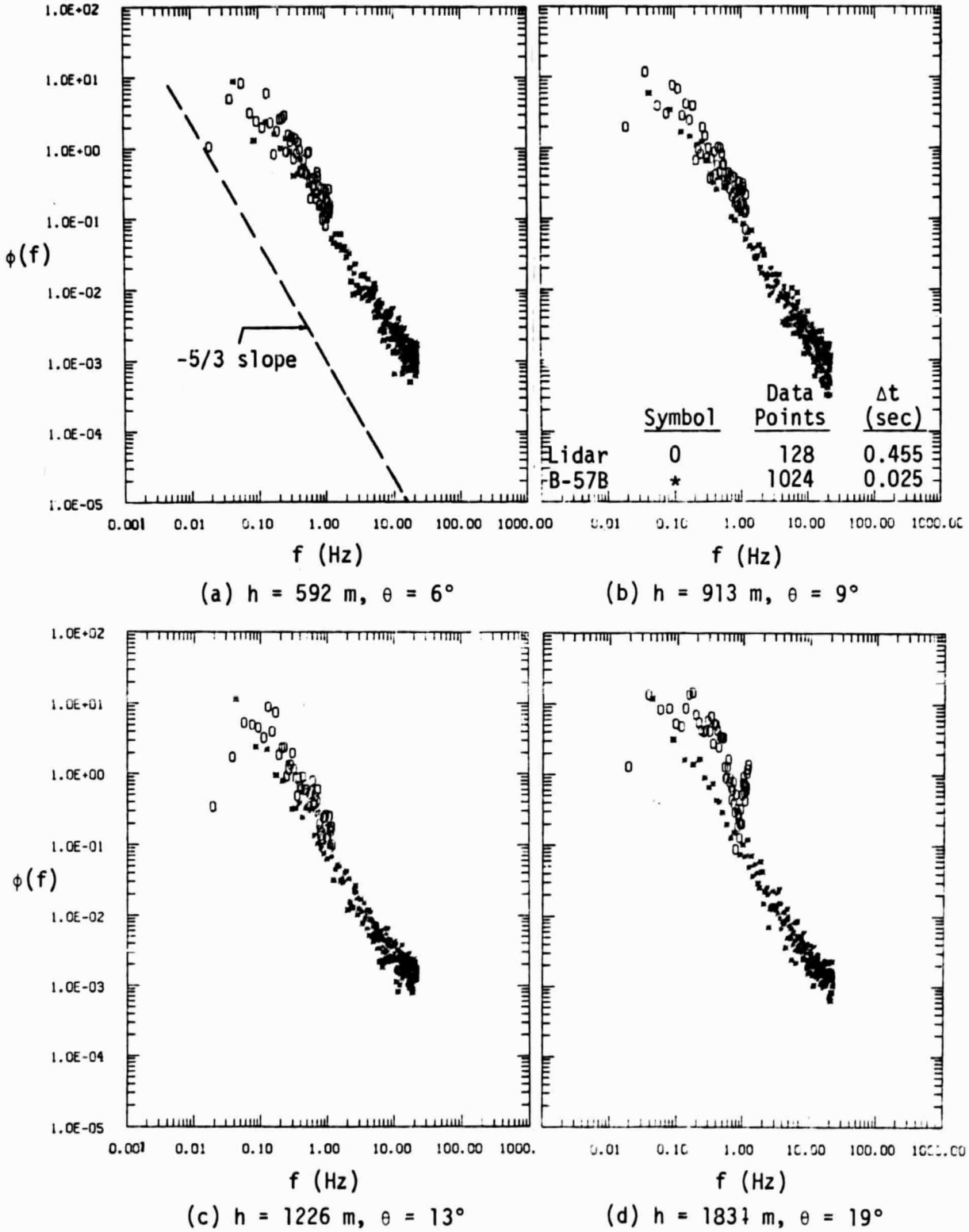

Figure 3.7. Comparison of radial turbulence spectra computed from aircraft and lidar measurements.

short for this particular run (as shown in Figure 3.4d) or due to decreasing SNR at the higher range gates (#18). Figure 3.7 also shows that, generally speaking, the spectra distributions of both aircraft- and lidar-measured turbulence follow a -5/3 slope for the inertia subrange, which is a typical finding for atmospheric turbulence.

3.2 Lidar Amplitude Related to Turbulence Intensity

As mentioned in the previous report (Frost and Huang 1983), the computed turbulence intensity for lidar-measured winds is extremely uncertain at the higher elevations (or higher range gates). Therefore, an effort was made in this study to determine if a calibration existed between turbulence intensity and lidar signal amplitude (or lidar signal intensity). Data from May 12, 1983, were utilized to investigate if such a relationship exists. Figure 3.8 is a plot of turbulence intensity versus lidar signal amplitude.

The independent variable is the lidar amplitude as provided on the NASA/MSFC lidar data tapes. The dependent variable in Figure 3.8 is the ratio of turbulence intensity calculated from the time histories of the radial velocity from the lidar to that of the B-57B aircraft, respectively. Assuming that the B-57B measures the real turbulence intensity, a relationship between lidar-calculated turbulence and lidar amplitude would provide a correction factor for adjusting σ_{Lidar}. Figure 3.8 suggests that a functional relationship of the form $\sigma_{Lidar}/\sigma_{Aircraft} = f(amp)$ may exist. Plotted in the figure are composites of eight runs. Data for each specific run is indicated by the number at the data positions. The figure contains data from only range gates 9 through 18.

Applying a curve fit routine, the calibration formula is found to be:

$$f(amp) = \begin{cases} e^{0.11\ (amp-50)} & amp \geq 50\ db \\ 1 & amp < 50\ db \end{cases}$$

An inherent assumption, however, is that there is no variation in the aerosol content over the altitude interval investigated. If there is a

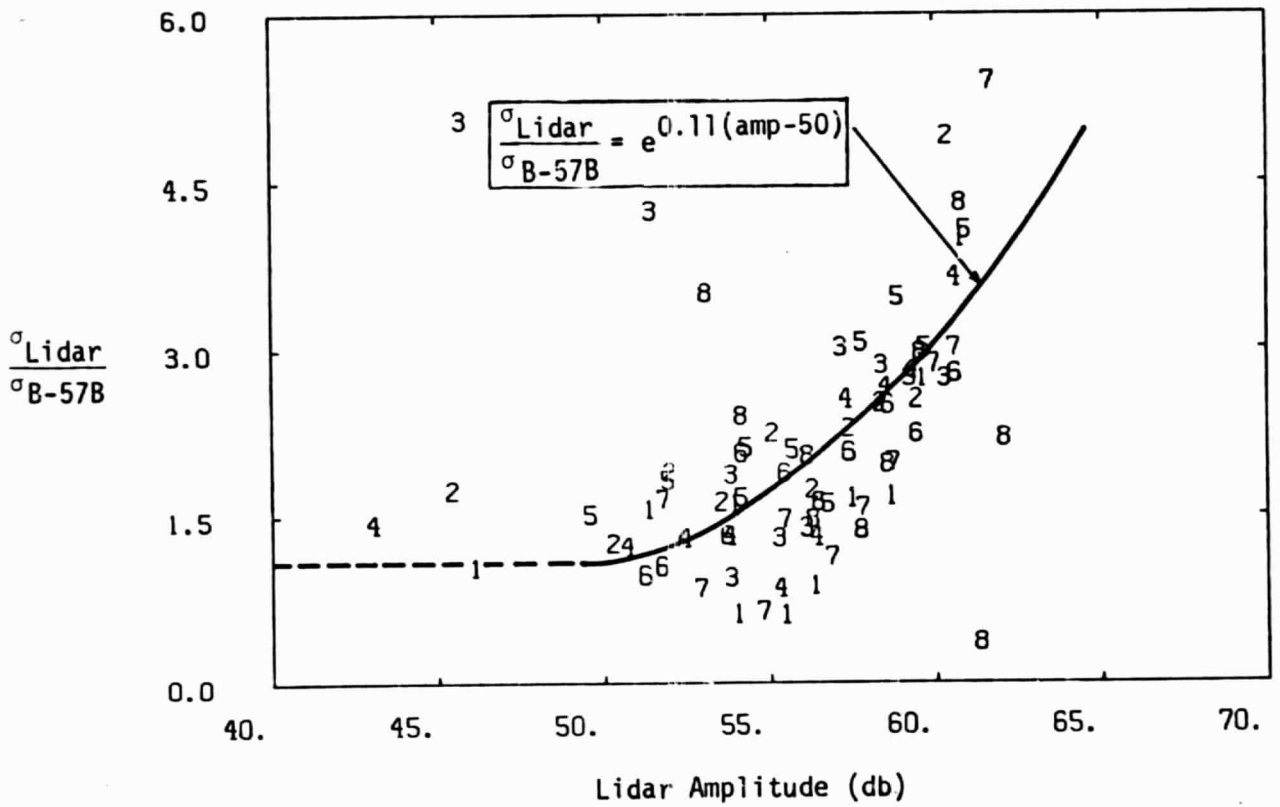

Figure 3.8. Relation between lidar amplitudes and turbulence intensities.

strong relation between lidar amplitude and aerosol content, Figure 3.8 may be simply illustrating that phenomenon. In order to establish confidence in the potential relationship between lidar amplitude and turbulence intensity, further studies are required.

3.3 NOAA/WPL Field Test

The field test carried out in Boulder was similar to the May 12, 1983, test at NASA/MSFC as indicated in Section 2.2. The method used to analyze these data was the same as the method indicated in a previous report (Frost and Huang 1983). The experiment was a two-day test, i.e., February 7 and 9, 1984. The aircraft flew a total of 16 paths, including 8 approaches along the 20° azimuth (parallel to 200° azimuth lidar beam) and 8 climbouts along 290° azimuth for each day. However, only six runs of the February 7 flight and four runs of the February 9 flight overlapped with lidar measurement, as shown in Tables 3.1 and 3.2. Figures 3.9 and 3.10 show the wind vector for both days. It clearly shows that the prevailing wind on February 7 was blowing toward the mountain while it was blowing from the mountain on February 9. Some of the flight trajectories appear to be far from the lidar beam which again is believed to be the INS drift problem. The lidar-measured wind in each range gate is a spatial average over the 300 m length of the sample volume (2 μs pulse duration). The time history of the aircraft-measured wind is then averaged over a period corresponding to the length of time required for the aircraft to traverse the 300 m range gate along the flight path. As indicated in the previous report, two approaches to carrying out this averaging technique were adopted. One was to assume vertical homogeneity in the flow field as shown in Figure 3.11a and the other technique was to average the wind assuming horizontal homogeneity as shown in Figure 3.11b.

Figures 3.12 and 3.13 compare the lidar-measured mean radial wind velocity with the aircraft-measured winds averaged over the corresponding 300 m sample volume, assuming horizontal homogeneity at 20° azimuth and 290° azimuth, respectively. Figures 3.14 and 3.15 show the same comparison except assuming vertical homogeneity. It was difficult to find two

TABLE 3.1. Selected Runs of the February 7 Test.

B-57B Aircraft Data			NOAA Lidar Data		
Run No.	Azimuth Angle	Sampling Time (MST) Start to End	PRF (Hz)	Number of Pulse Average	Sampling Time (MST) Start to End
2	290	11:46:42-11:49:19	12	6	11:46:53-11:49:04
3	200	11:56:42-12:00:27	12	6	11:57:59-12:00:06
4	290	12:02:03-12:03:59	12	6	12:00:50-12:02:55
5	200	12:12:01-12:15:56	12	6	12:12:17-12:16:41
6	290	12:17:48-12:21:29	12	6	12:16:43-12:19:50
7	200	12:27:51-12:31:49	12	6	12:27:00-12:29:35

TABLE 3.2. Selected Runs of the February 9 Test.

B-57B Aircraft Data			NOAA Lidar Data		
Run No.	Azimuth Angle	Sampling Time (MST) Start to End	PRF (Hz)	Number of Pulse Average	Sampling Time (MST) Start to End
9	200	12:14:06-12:17:45	12	48	12:13:39-12:17:23
10	290	12:19:30-12:23:09	12	24	12:17:45-12:22:13
11	200	12:28:05-12:31:43	12	24	12:28:49-12:30:53
12	290	12:33:25-12:37:09	12	24	12:33:47-12:36:49

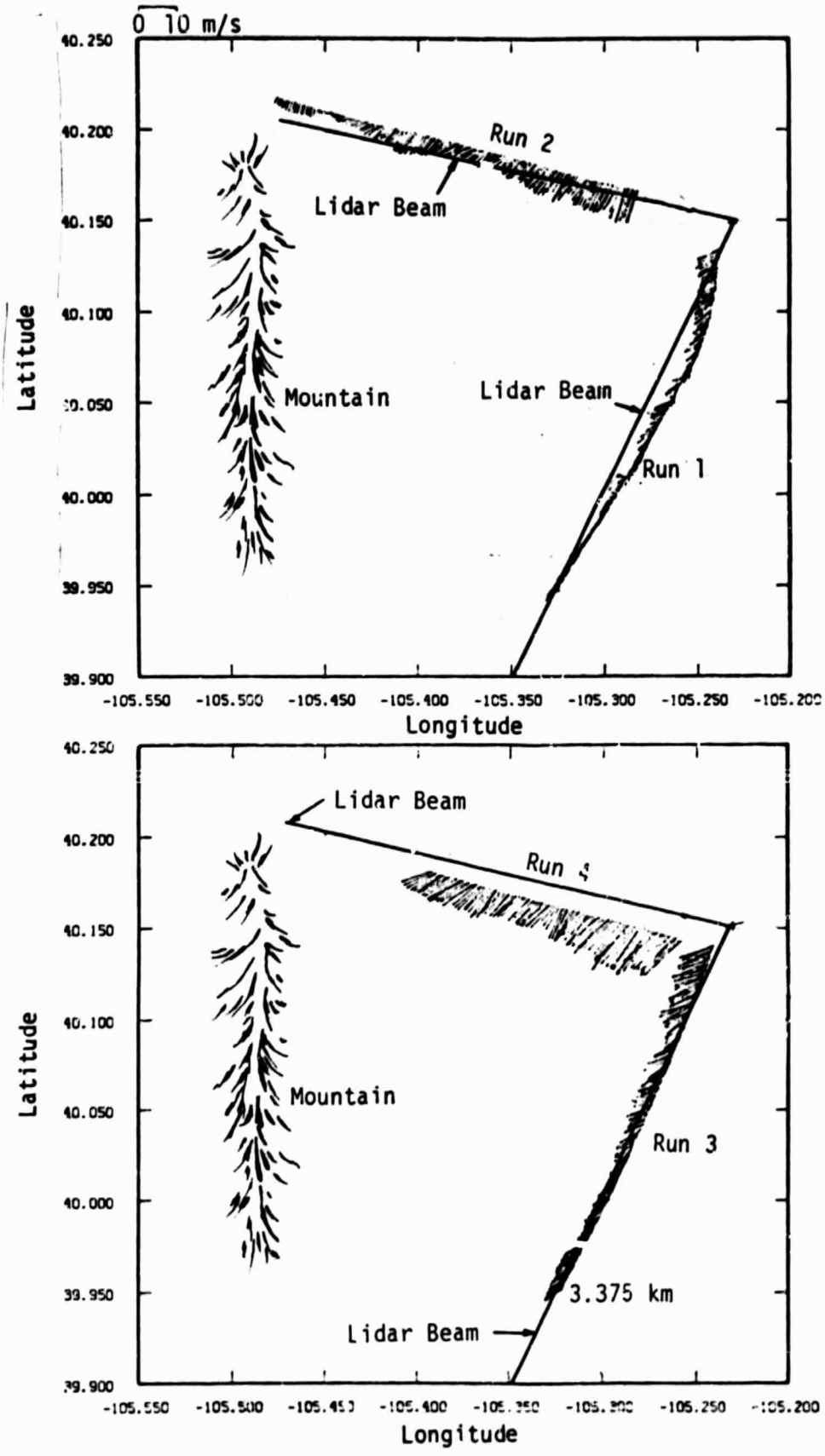

Figure 3.9. Aircraft-measured wind vector on February 7 flight.

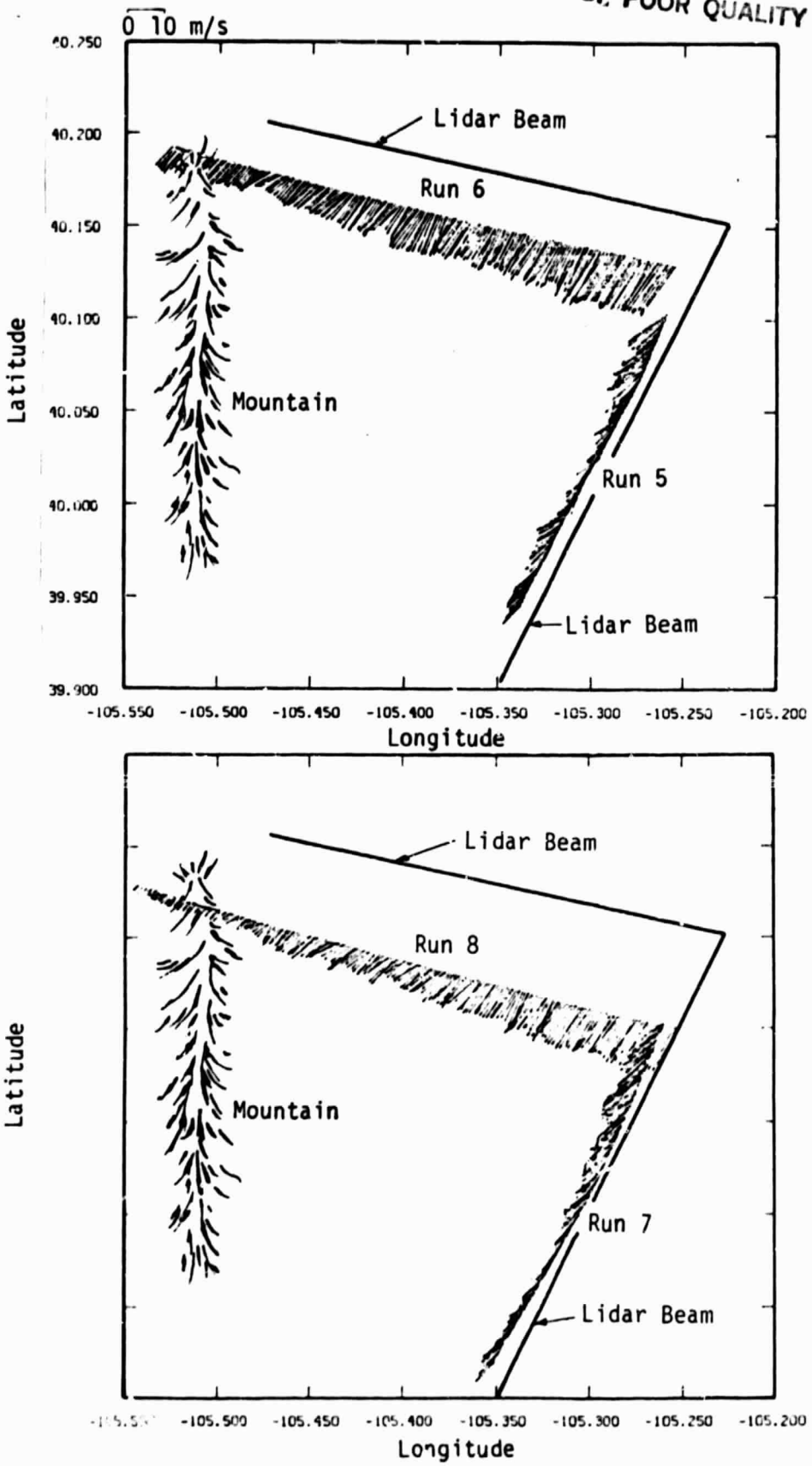

Figure 3.9. (continued).

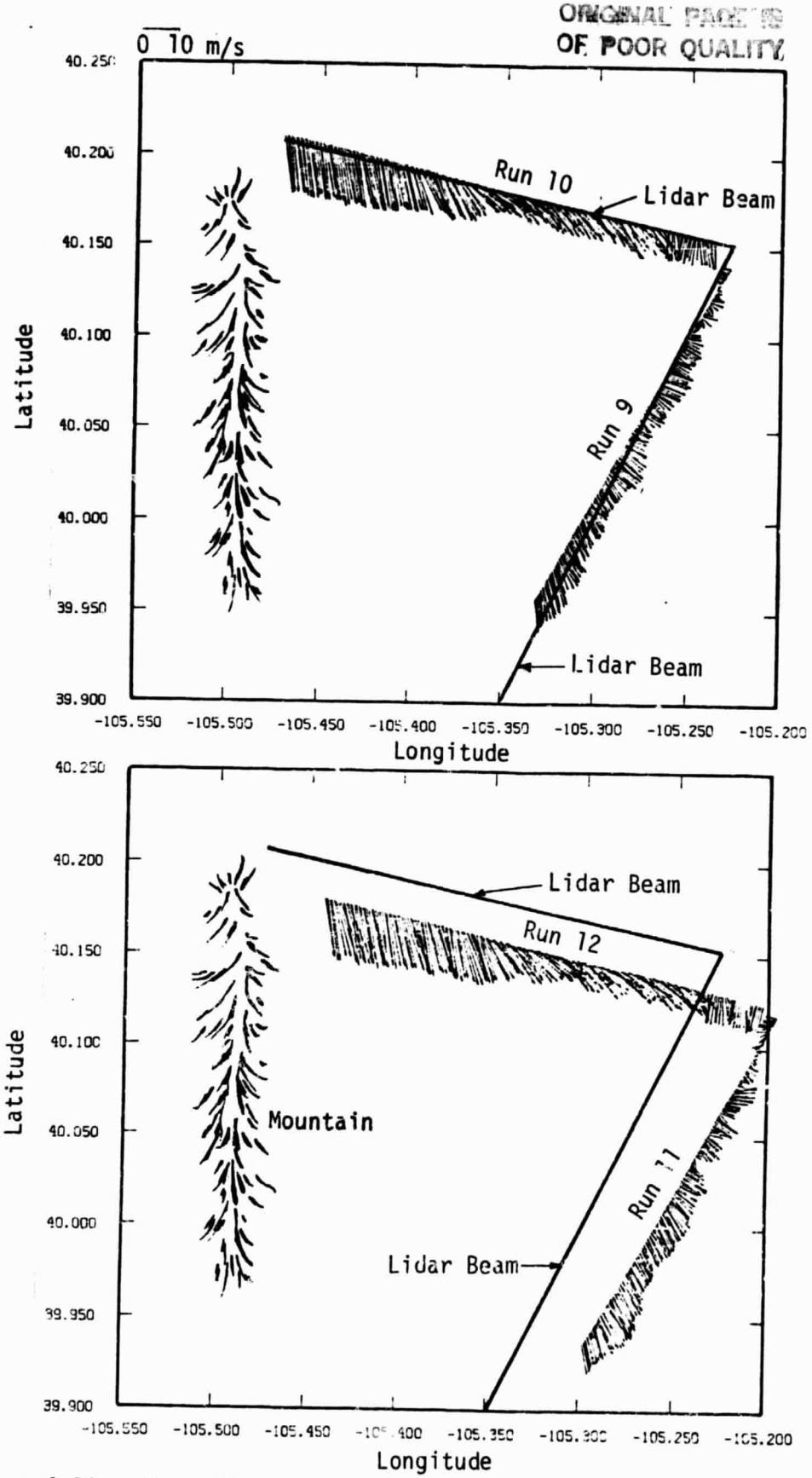

Figure 3.10. Aircraft-measured wind vector on February 9 flight.

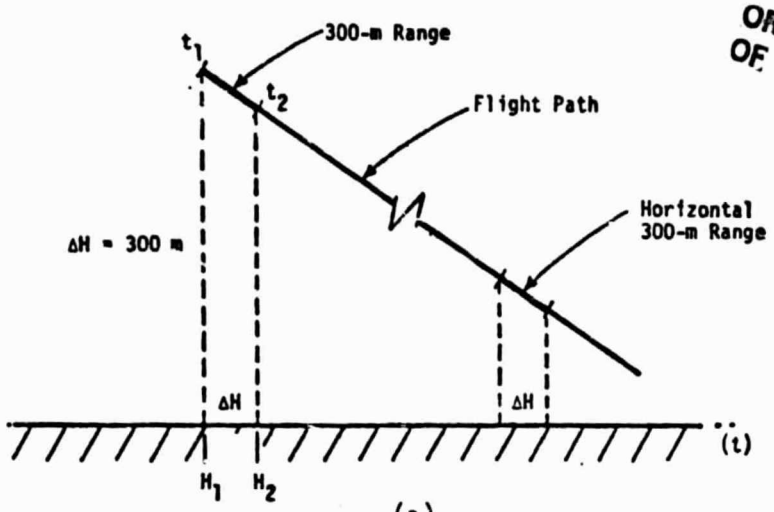

(a)

$$\bar{W} = \frac{1}{(N_2 - N_1 + 1)} \sum_{i=N_1}^{N_2} w_i$$

$$N_1 = \frac{t_1 - t_0}{0.025} \qquad N_2 = \frac{t_2 - t_0}{0.025}$$

t_0 = beginning of each run

t_1 = time airplane enters each horizontal range at H_1

t_2 = time airplane leaves each horizontal range at H_2

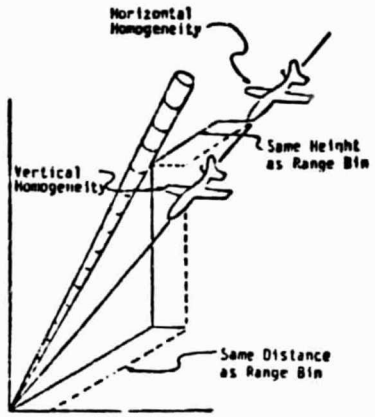

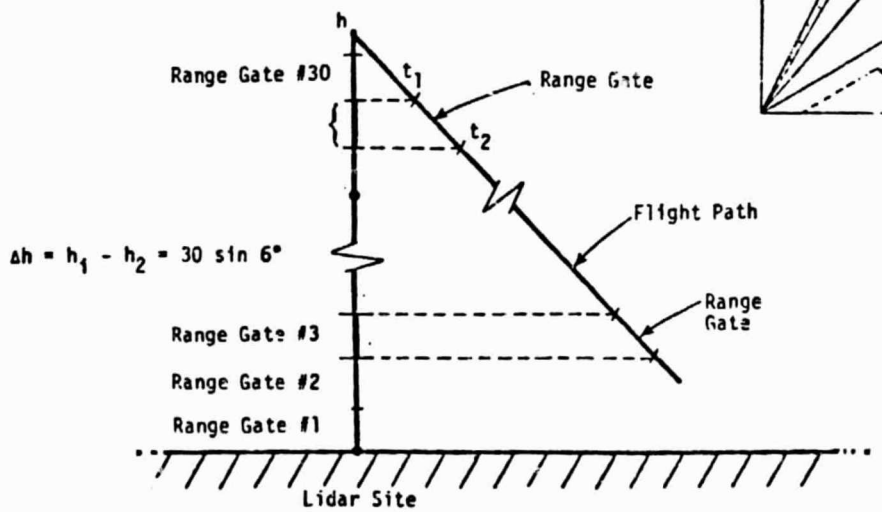

$\Delta h = h_1 - h_2 = 30 \sin 6°$

(b)

$$\bar{W} = \frac{1}{(N_2 - N_1 + 1)} \sum_{i=N_1}^{N_2} w_i$$

$$N_1 = \frac{t_1 - t_0}{0.025} \qquad N_2 = \frac{t_2 - t_0}{0.025}$$

t_0 = beginning of each run

t_1 = time airplane enters each range gate at height h_1

t_2 = time airplane leaves each range gate at height h_2

Figure 3.11. Evaluation procedure for averaging B-57B wind for each range gate.

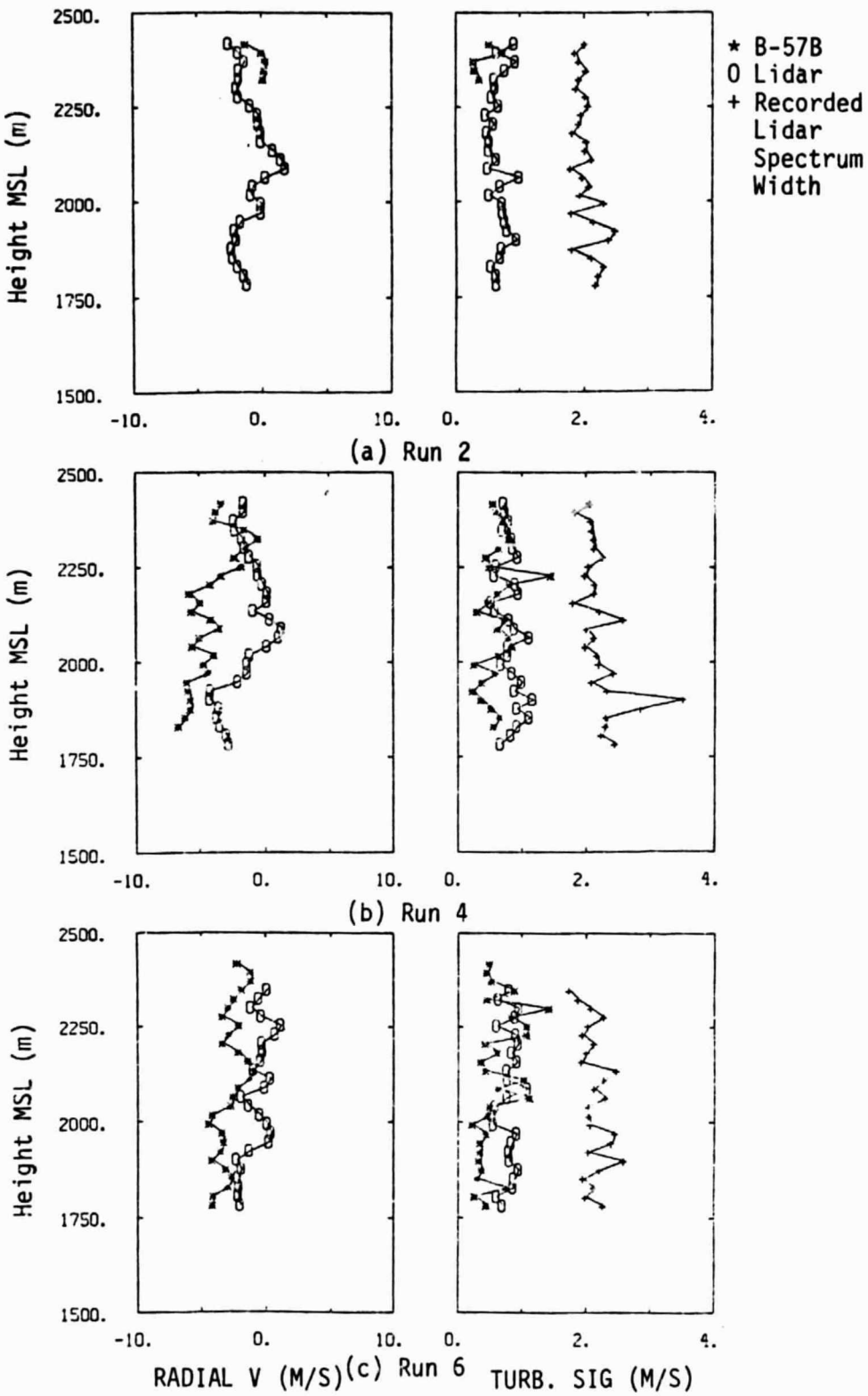

Figure 3.12. Comparison of radial mean wind velocity, calculated turbulence intensity, and lidar spectral width between aircraft measurement and lidar measurement on February 7, 1984 (290° azimuth assuming horizontal homogeneity).

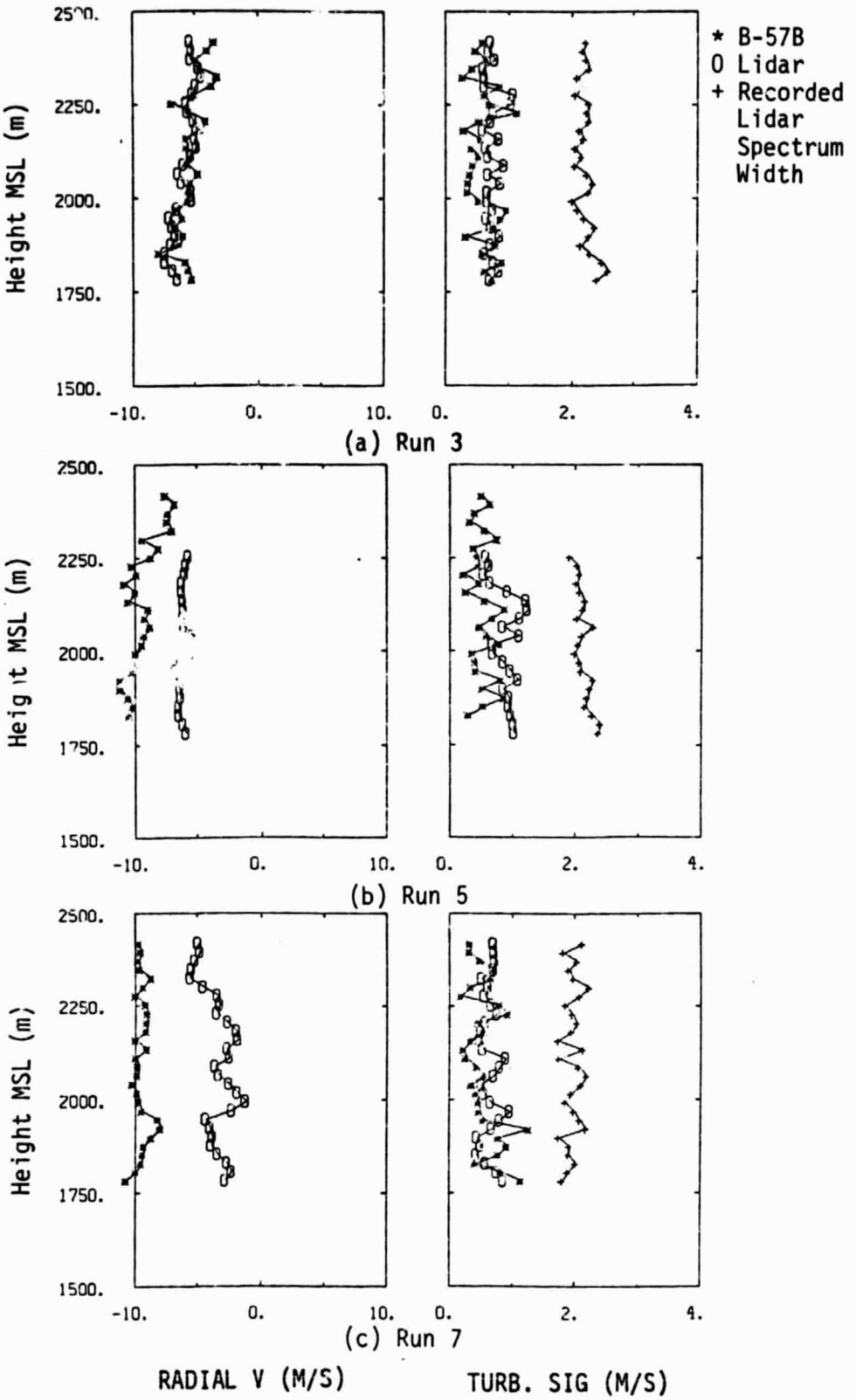

Figure 3.13. Comparison of radial mean wind velocity, calculated turbulence intensity, and lidar spectral width between aircraft measurement and lidar measurement on February 7, 1984 (20° azimuth assuming horizontal homogeneity).

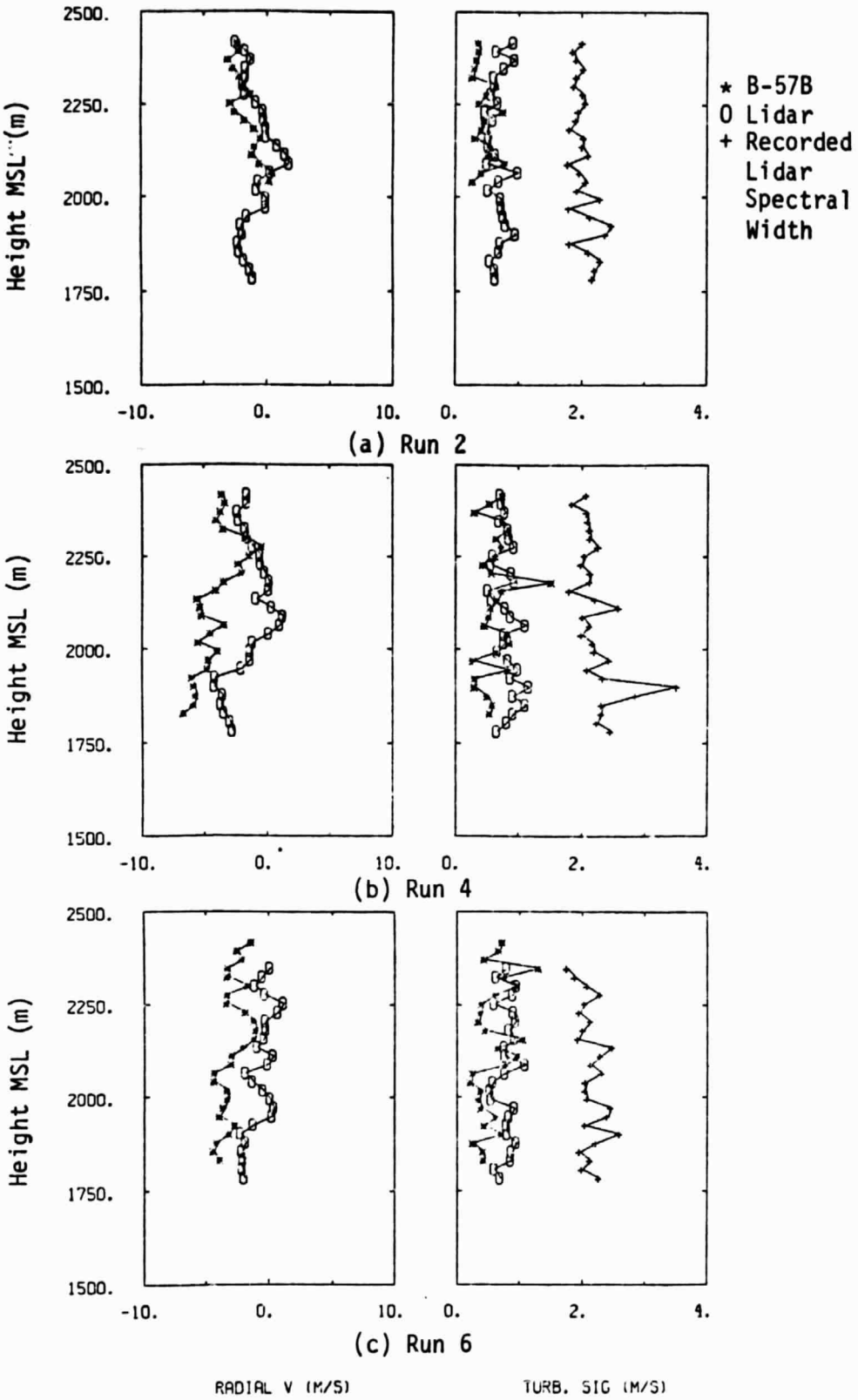

Figure 3.14. Comparison of radial mean wind velocity, calculated turbulence intensity, and lidar spectral width between aircraft measurement and lidar measurement on February 7, 1984 (290° azimuth assuming vertical homogeneity).

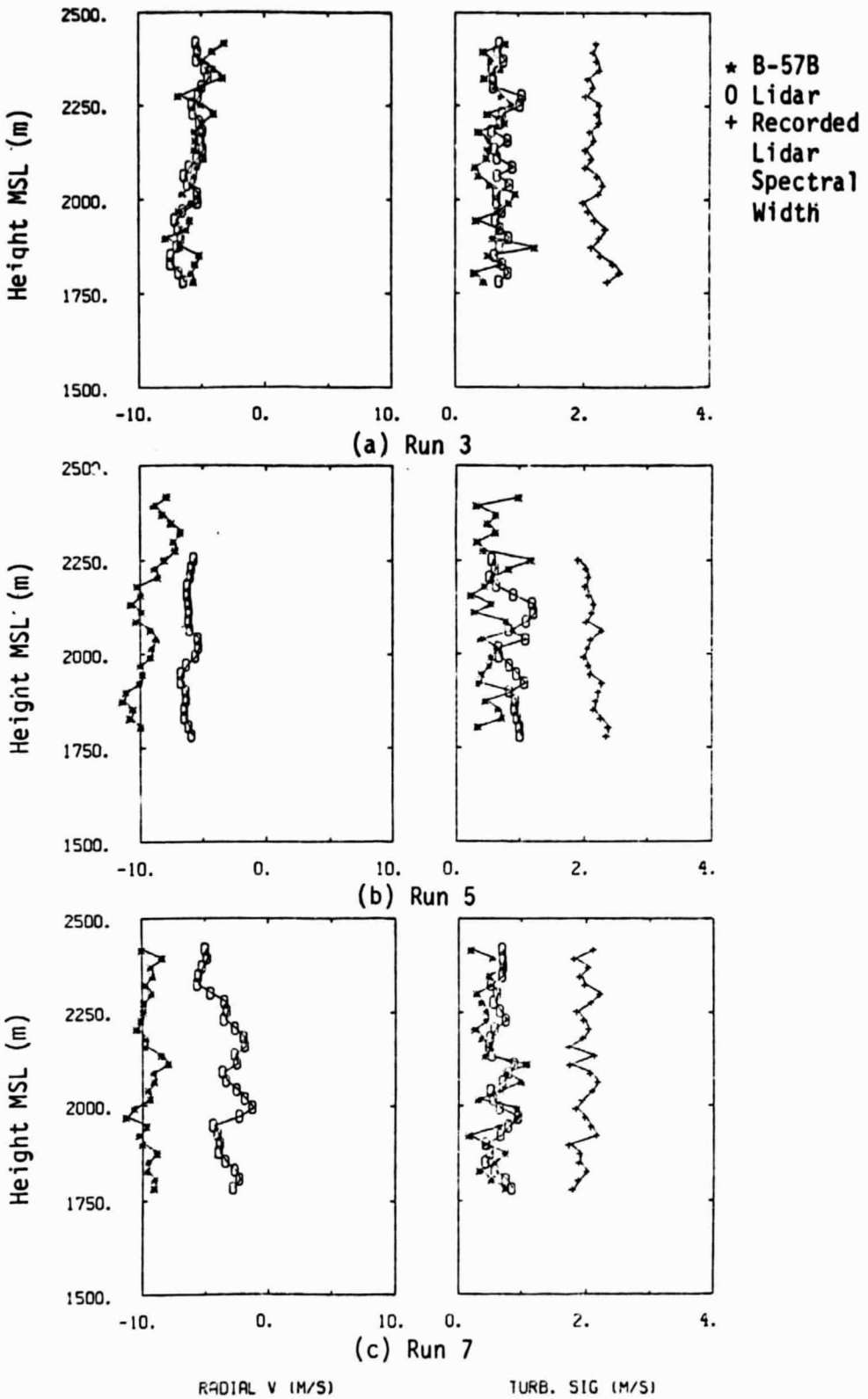

Figure 3.15. Comparison of radial mean wind velocity, calculated turbulence intensity, and lidar spectral width between aircraft measurement and lidar measurement on February 7, 1984 (20° azimuth assuming vertical homogeneity).

corresponding sampling volumes to compare under the assumption of vertical homogeneity, when the recorded aircraft coordinates are questionable (due to INS drift problem). However, a reasonable guess was made to adjust the aircraft trajectories. By comparing Figure 3.12 with Figure 3.14 and Figure 3.13 with Figure 3.15, there is no significant difference between the two methods of comparison (i.e., assuming either horizontal homogeneity or vertical homogeneity).

Since the mean wind direction on February 7 is 30° from true north, the magnitude of wind speed at 20° azimuth is higher than that at 290° (comparing Figure 3.12 and 3.13). The negative radial wind speed means the wind was away from the lidar site. Differences of radial mean wind speed between aircraft measurement and lidar measurement are noticed in these figures (Figure 3.12 to 3.15). It was also noticed that the magnitude of aircraft-measured wind was larger than the lidar-measured wind in most cases. One possibility is inaccuracy in wind measurements due to the Schuler frequency of the aircraft navigation system or due to variation in pulse transmission frequency of the lidar system. Despite the difference of mean wind from both measurements, the turbulence intensities measured by computing the lidar wind time history for each range gate agree very well with aircraft-measured intensity during the interval the aircraft is passing through the range gate. The outputs of the second moment (lidar spectra width) are also available for the NOAA/WPL lidar system. However, the magnitude of spectral width is in the range of 2 to 3 m/s, which is 4 to 5 times the actual turbulence intensity. It is believed that the major contribution of these large spectral width values is the broadening of the square pulse itself in the spectrum estimator. Careful investigation of the signal process needs to be carried out to resolve the correlation between lidar spectral width and turbulence intensity.

Data of February 9 are also examined. Figure 3.16 and 3.17 show the comparision of both measurements at different azimuth angle, i.e., 290° and 20°, respectively. From both runs of Figure 3.16, the reverse flow clearly appeared at slightly below 2000 m. This flow phemonenon only

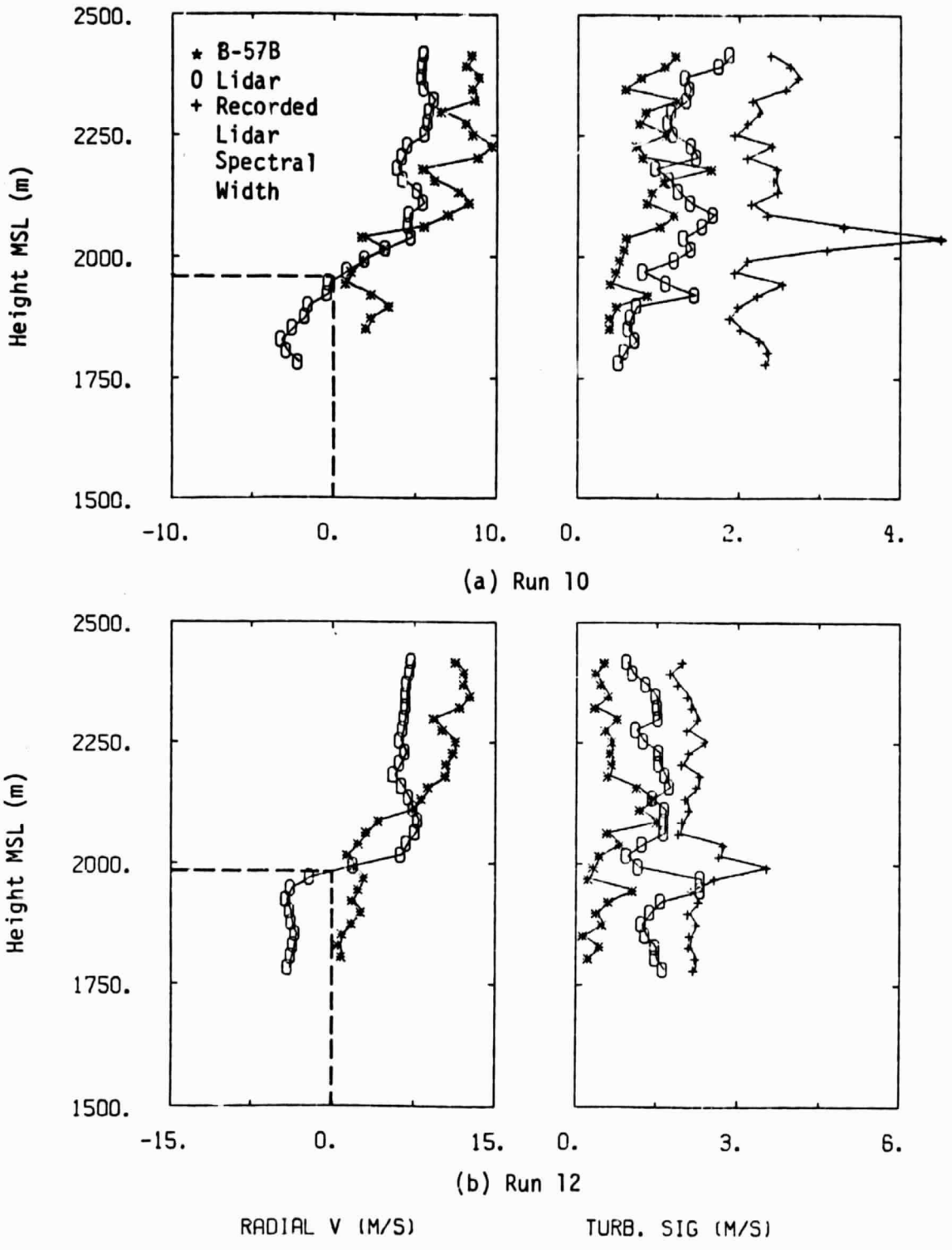

Figure 3.16. Comparison of radial mean wind velocity, calculated turbulence intensity, and lidar spectral width between aircraft measurement and lidar measurement on February 9, 1984 (290° azimuth assuming horizontal homogeneity).

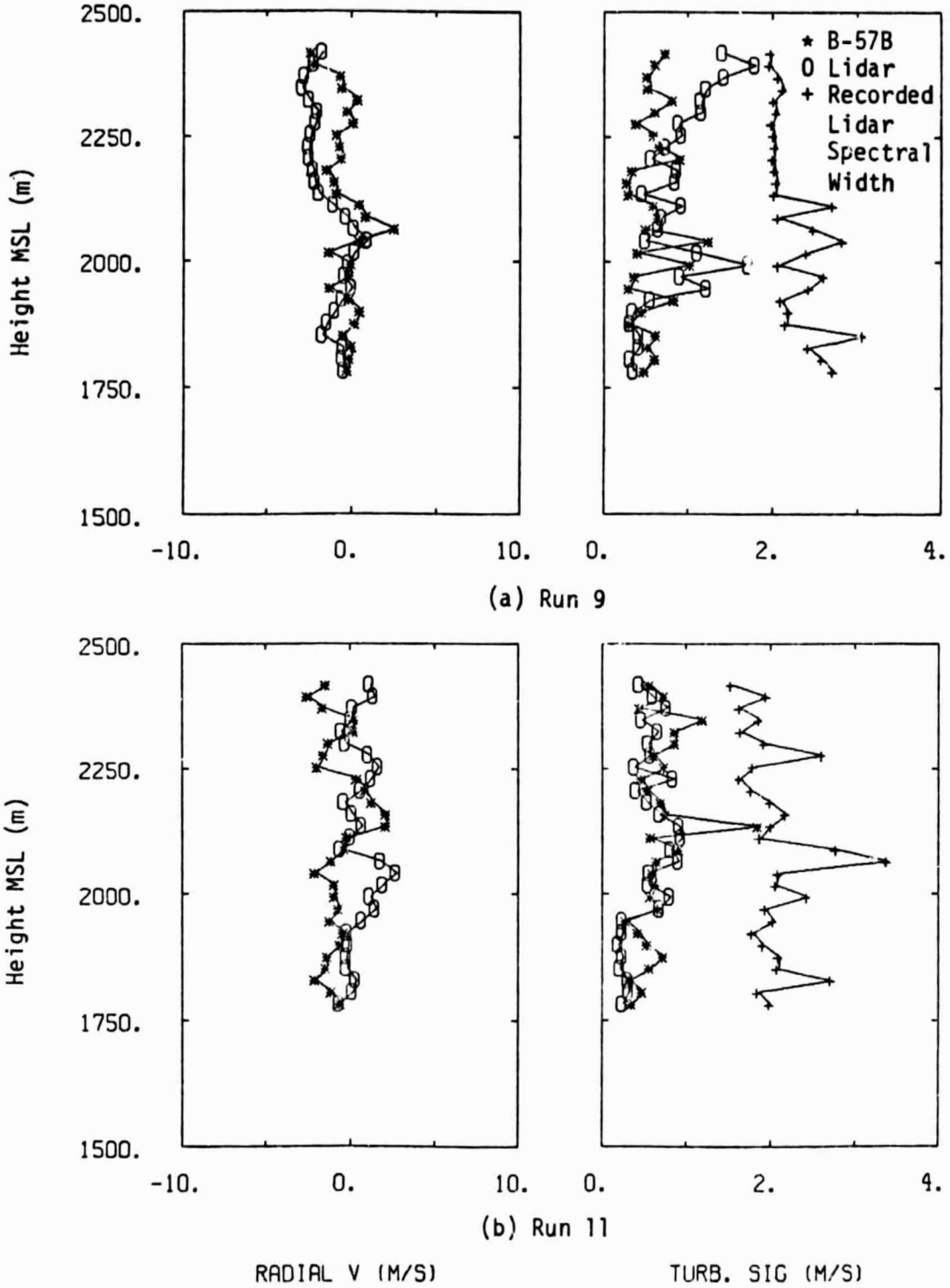

Figure 3.17. Comparison of radial mean wind velocity, calculated turbulence intensity, and lidar spectral width between aircraft measurement and lidar measurement on February 9, 1984 (20° azimuth assuming horizontal homogeneity).

appears at the direction roughly perpendicular to the mountain range and is not seen in Figure 3.17 which is 20° azimuth or on February 7 when the prevailing wind direction is 30° toward the mountain range. Similar flow patterns were detected by B-57B measurements during the turbulent flux measurements portion of the orographic campaign (Theon 1985).

Turbulence intensities from the February 9 data were also computed from aircraft-measured wind and lidar-measured wind. As indicated in Table 3.2, the number of pulses averaged are 24 or 48 for lidar data while pulse repetition frequency is 12 Hz. The time interval between two sequential outputs is 2 or 4 seconds. A significant loss of turbulence information could occur due to long time period averaging. Although the spectral widths are still higher than computed turbulence intensities, it is interesting to see that the variation of lidar spectral width is strongly correlated with the wind shear. As shown in Figure 3.16, a strong wind shear occurred slightly above 2000 m altitude for both Runs 10 and 12 and a larger value of spectral width appeared at the same altitude for both runs.

Turbulence spectra were computed for each of six flight paths (three in 290° azimuth and three in 20° azimuth) and at each corresponding range gate, assuming horizontal homogeneity. The spectra computed for each range gate for the three flights in 290° and three flights in 20° were then segment averaged, respectively. Figure 3.18 shows the calculated turbulence spectra of some of the range gates for the 290° azimuth paths while Figure 3.19 shows results for the 20° azimuth paths. Note that the February 7 lidar data are sampled at two times per second resulting in a Nyquist frequency of 1 Hz. The aircraft data, on the other hand, are sampled at 40 times per second resulting in a Nyquist frequency of 20 Hz. The differences of sampling rate and the length of data resulted in the spectra falling on different frequency bands; the spectra, however, do merge at intermediate frequency values forming a relatively continuous line and follow the -5/3 slope quite well. Thus, the turbulence measured by both instruments displayed highly realistic features of natural turbulence structure.

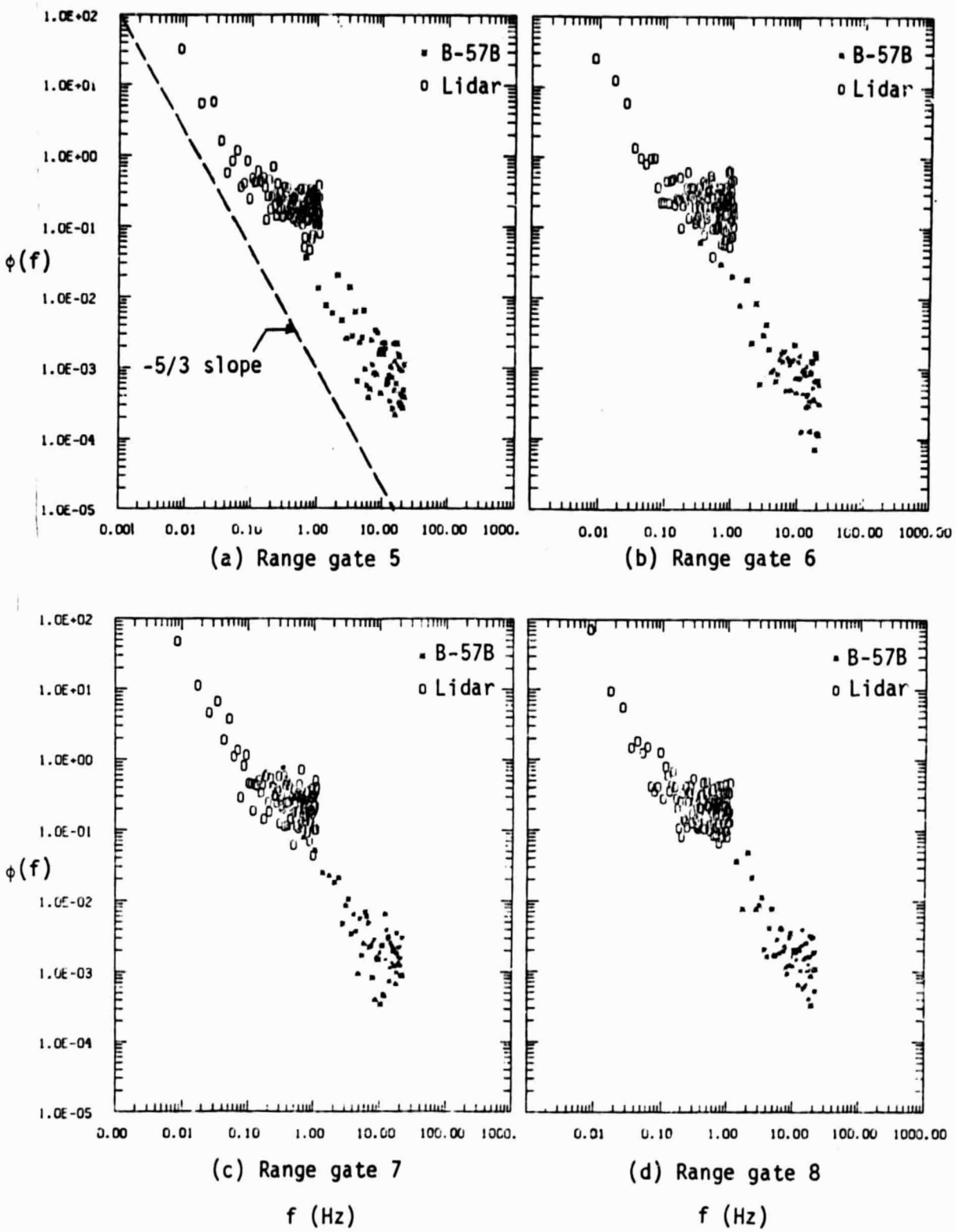

Figure 3.18. Computed turbulence spectral at 290° azimuth path.

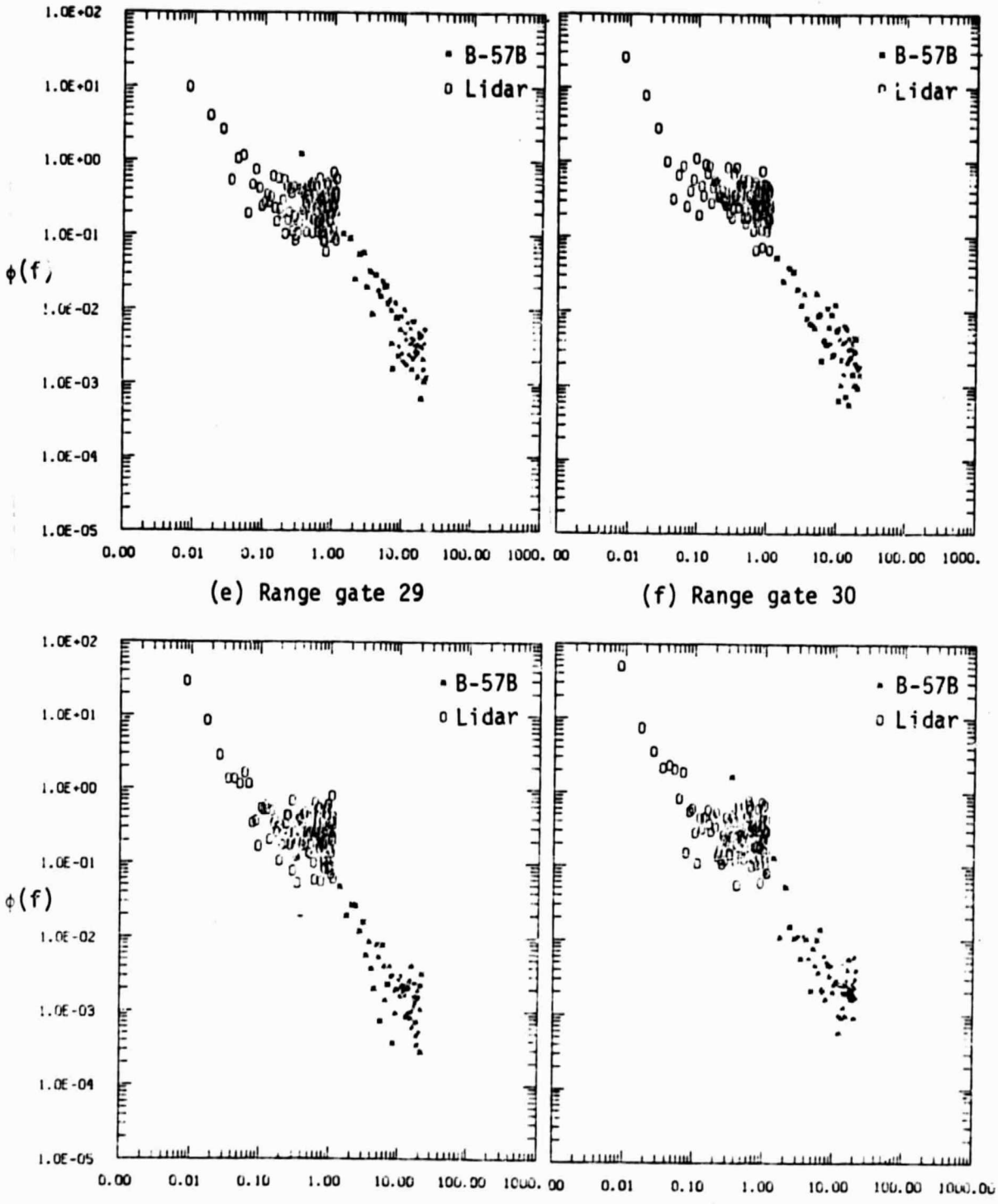

Figure 3.18. (continued).

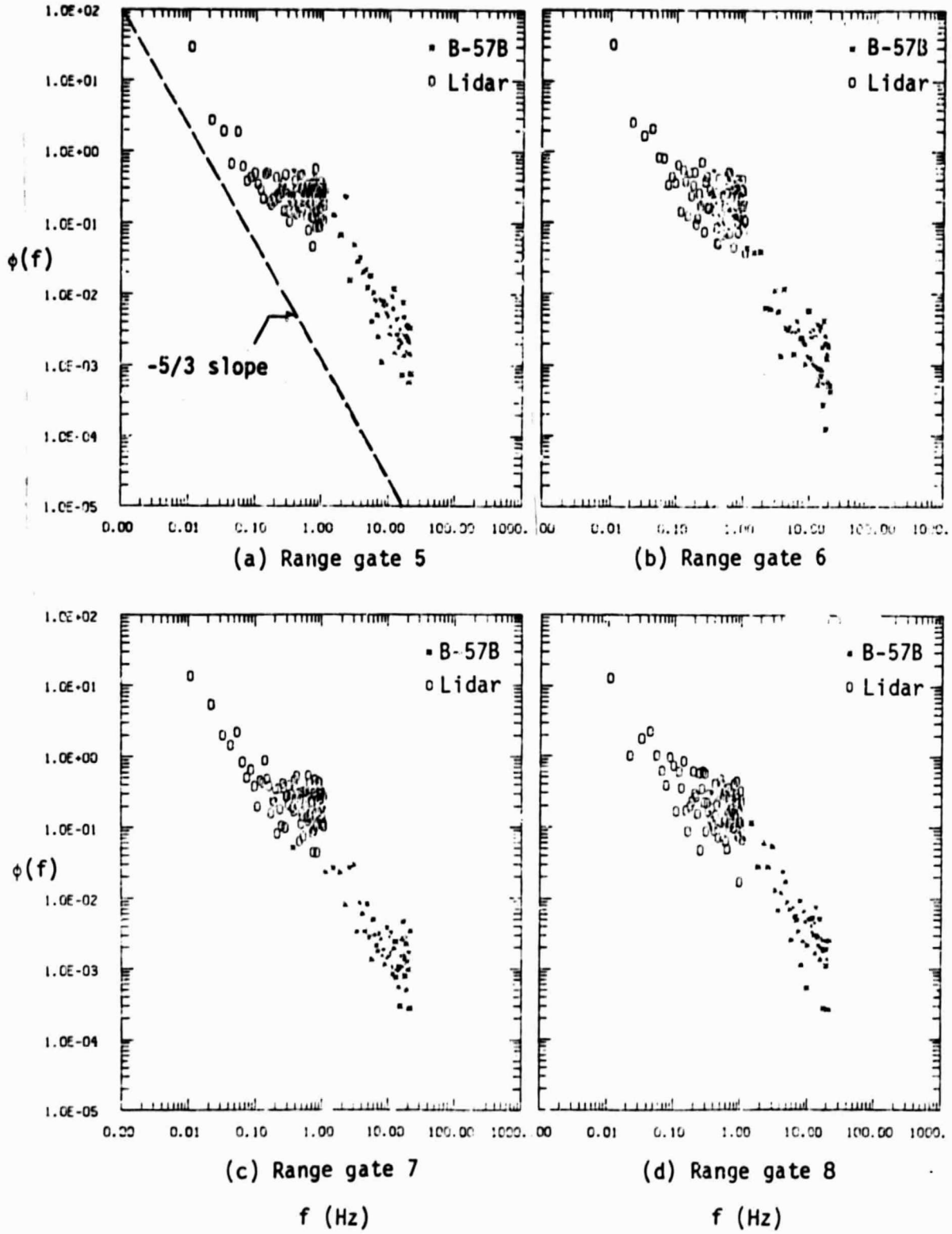

Figure 3.19. Computed radial turbulence spectra at 20° azimuth path.

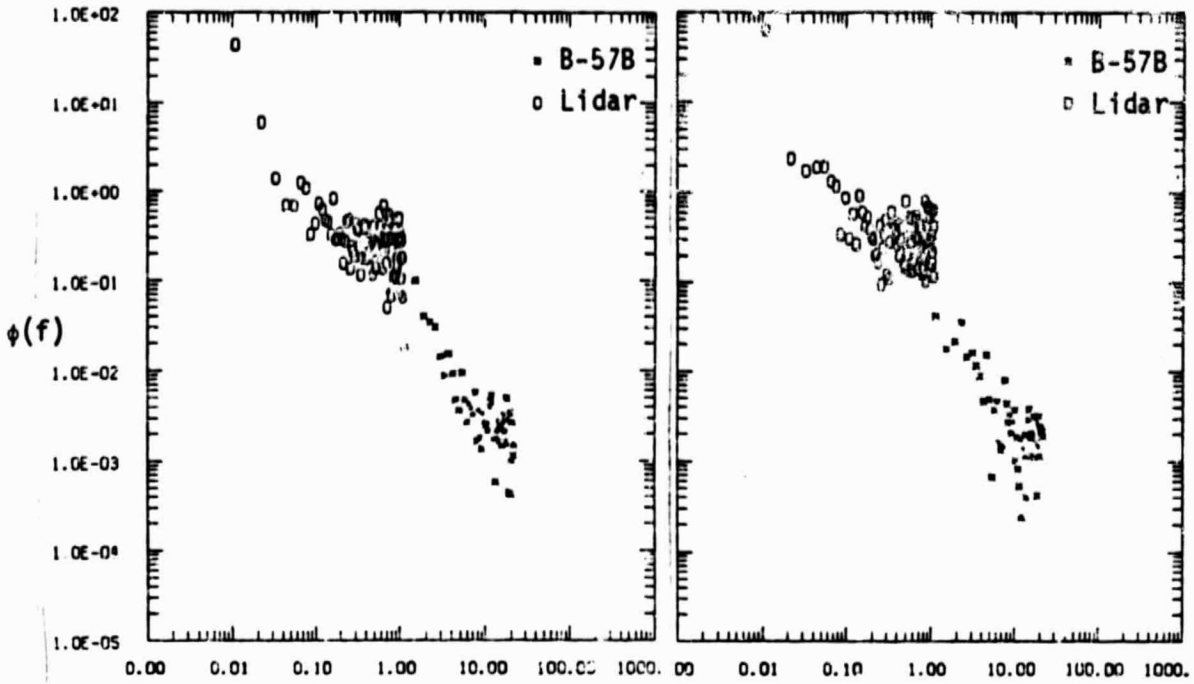

(e) Range gate 29

(f) Range gate 30

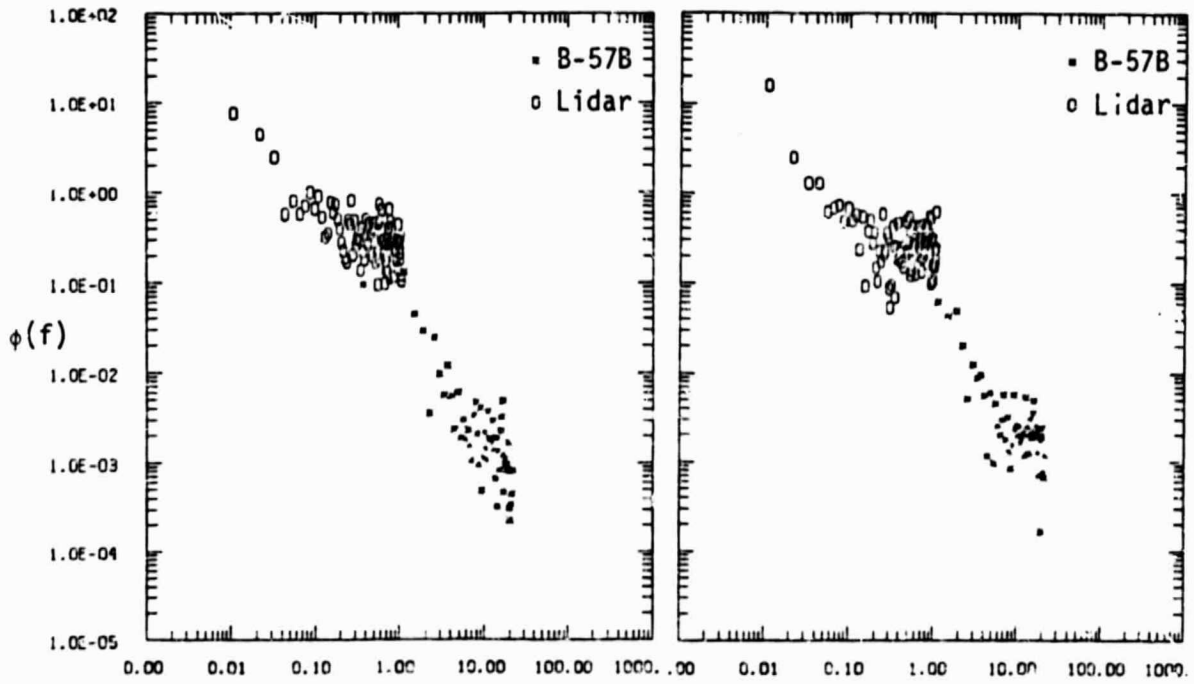

(g) Range gate 31

(h) Range gate 32

f (Hz)

f (Hz)

Figure 3.19. (continued).

4.0 CONCLUSIONS

The results of this study show general agreement between winds measured with the Doppler lidar and winds measured with the B-57B instrumented aircraft. In all comparisons the winds along the lidar beam and those measured along the aircraft flight path are in agreement within a factor of 10. In many cases, the agreement is much better and well within ±2 to 4 m/s. It is obvious that exact agreement between wind fields cannot be expected for a number of reasons: (1) the aircraft never flies exactly the same path as the lidar beam, (2) the lidar measurement is averaging the wind along a cylindrical volume element 500 m in extent whereas the aircraft represents a spatial average based on Taylor's hypothesis, (3) the aircraft measurements themselves have inaccuracy due to such factors as the Schuler frequency of the aircraft's INS, (4) the NOAA lidar was reported at the time of the experiment to have variations in pulse transmission frequency which also could induce inaccuracies in wind measurements. In view of all these factors, it is concluded that the lidar and aircraft measurements essentially show valid wind speed measurements.

Turbulence intensities measured by computing the lidar wind time history for each range gate and then calculating the rms value relative to the mean agree quite well with the aircraft intensities. The spectral width or second moment data from the lidar, however, does not correspond well with the aircraft-measured intensities being consistently a factor of 2 higher. This difference may be due to the natural pulse itself broadening the spectral estimator.

The computed spectra from lidar measurements fit the spectra computed from aircraft measurement values very well. Also, they follow an approximate -5/3 power law as is expected for turbulence in the atmosphere. The scatter in the spectral data is quite large but this is to be expected because of the small amounts of data used in the statistical averaging. The general results of the study, however, suggest that turbulence measurements with Doppler lidar systems holds considerable

promise. Further work in this area of comparing remote sensed values with *in situ* measurements is needed, however, to fully resolve the reliability of lidar-measured turbulence values.

REFERENCES

Bilbro, J. W. (1980). "Atmospheric Laser Doppler Velocimetry: An Overview," Optical Engineering, July-August issue, 19(4):533-542.

Bilbro, J. W., and W. W. Vaughan (1978): "Wind Field Measurement in The Nonprecipitous Regions Surrounding Severe Storms by an Airborne Pulsed Doppler Lidar System," Bull. of the Am. Met. Soc., 59(9):1095.

Brashears, M. R., and J. N. Hallock (1976). "The Measurement of Wind Shear and Wake Vortices by Laser Doppler Velocimetry," Seventh Conference on Aerospace and Aeronautical Meteorology and Symposium on Remote Sensing from Satellites, Melbourne, Fla., November.

Camp, D. W., W. Campbell, W. Frost, H. Murrow, and W. Painter (1983). "NASA's B-57B Gust Gradient Program," AIAA Paper No. 83-0208, Presented at the AIAA 21sth Aerospace Sciences Meeting, Reno, Nevada, January.

Campbell, W., D. W. Camp, and W. Frost (1983). "An Analysis of Spanwise Gust Gradient Data," Preprints: Ninth Conference on Aerospace and Aeronautical Meteorology, June 6-9, Omaha, Neb., Am. Met. Society, Boston, Mass.

Cliff, W. C., and R. M. Huffaker (1974). "Application of a Single Laser Doppler System to the Measurement of Atmospheric Winds," NASA TMX-64891, October.

Cook, N. J., B. H. Coulson, and W. McKay (1978). "Wind Conditions Around the Rock of Gibraltar," Journal of Industrial Aerodynamics, 2:289-309.

Frost, W., and K. H. Huang (1983). "Doppler Lidar Signal and Turbulence Study," Final report for NASA/MSFC under Contract NAS8-35185 by FWG Associates, Inc., Tullahoma, Tenn., December

Hall, F. F., R. M. Huffaker, R. M. Hardesty, M. E. Jackson, T. R. Lawrence, M. J. Post, R. A. Richter, and B. F. Weber (1984). "Wind Measurement Accuracy of the NOAA Pulsed Infrared Doppler Lidar," Applied Optics, 23(15), August.

Huffaker, R. M. A. Jelalian, J. A. L. Thomson (1970). "Laser-Doppler System for Detection of Aircraft Trailing Vortices," Proc. IEEE, 58:322, March.

Jeffreys, H. B., and J. W. Bilbro (1975). "Development of a Laser Doppler System for the Detection and Monitoring of Atmospheric Disturbances," NASA TM X-64981.

Lawrence, T. R., D. J. Wilson, C. E. Craven, I. P. Jones, R. M. Huffaker, and J. A. Thomson (1972). "Laser Velocimeter for Remote Sersing," Rev. Sci. Instrum., 43:512, November.

Lee, R. W. (1982). "NASA Airborne Doppler Lidar Program: Data Characteristics of 1981 Wind Field Measurements," Technical Report #1, Prepared for NASA/MSFC under Contract NAS8-34768 by Lassen Research, Manton, CA 96059.

Post, M. J. R. A. Richter, R. M. Hardesty, T. R. Lawrence, and F. F. Hall (1981). "National Oceanic and Atmospheric Administration's (NOAA) Pulsed, Coherent, Infrared Doppler Lidar--Characteristics and Data," SPIE Vol. 300, Physics and Technology of Coherent Infrared Radar.

Theon, J. S. (1985). "The Effects of Orography on Land-Atmosphere Turbulent Exchange Processes," Ph.D. Dissertation, University of Tennessee, March.